Am J Nucl Med Mol Imaging 2020;10(1):1-31
www.ajnmmi.us /ISSN:2160-8407/ajnmmi0108227

*Review Article*

# Imaging of intranasal drug delivery to the brain

Michael C Veronesi[1], Mosa Alhamami[1], Shelby B Miedema[1,2], Yeonhee Yun[1], Miguel Ruiz-Cardozo[3], Michael W Vannier[4]

*[1]Department of Radiology & Imaging Sciences, Indiana University School of Medicine, USA; [2]Department of Biomedical Engineering, Indiana University-Purdue University Indianapolis, USA; [3]Clinical Research Institute, Universidad Nacional de Colombia School of Medicine, USA; [4]Department of Radiology, University of Chicago School of Medicine, USA*

Received January 21, 2020; Accepted February 7, 2020; Epub February 25, 2020; Published February 28, 2020

**Abstract:** Intranasal (IN) delivery is a rapidly developing area for therapies with great potential for the treatment of central nervous system (CNS) diseases. Moreover, in vivo imaging is becoming an important part of therapy assessment, both clinically in humans and translationally in animals. IN drug delivery is an alIn fact, imaging hasternative to systemic administration that uses the direct anatomic pathway between the olfactory/trigeminal neuroepithelium of the nasal mucosa and the brain. Several drugs have already been approved for IN application, while others are undergoing development and testing. To better understand which imaging modalities are being used to assess IN delivery of therapeutics, we performed a literature search with the key words "Intranasal delivery" and "Imaging" and summarized these findings in the current review. While this review does not attempt to be fully comprehensive, we intend for the examples provided to allow a well-rounded picture of the imaging tools available to assess IN delivery, with an emphasis on the nose-to-brain delivery route. Examples of in vivo imaging, for both humans and animals, include magnetic resonance imaging (MRI), positron emission tomography (PET), single-photon emission computed tomography (SPECT), gamma scintigraphy and computed tomography (CT). Additionally, some in vivo optical imaging modalities, including bioluminescence and fluorescence, have been used more in experimental testing in animals. In this review, we introduce each imaging modality, how it is being utilized and outline its strengths and weaknesses, specifically in the context of IN delivery of therapeutics to the brain.

**Keywords:** Intranasal drug delivery, theranostics, multimodality imaging, blood-brain barrier

## Introduction

The blood-brain barrier (BBB) is highly successful at protecting the brain from entry of potentially detrimental substances. Unfortunately, greater than 99% of potential therapies are also greatly restricted from entering the brain [1, 2]. Therefore, there is an urgent need to develop alternative delivery strategies for getting therapies around the BBB non-invasively. Intranasal (IN) delivery is a promising alternative to systemic administration that uses the direct anatomic pathway between the olfactory/trigeminal neuroepithelium of the nasal mucosa and the brain. Since only small amounts of a drug are delivered to the brain using this route, the mechanism of delivery needs to be better understood and new methods need to be developed to overcome the obstacles facing nose-to-brain delivery of promising therapeutics. The key to overcoming these challenges and furthering the field of IN delivery is to develop informative, non-invasive methodologies to better understand the nose-to-brain delivery pathway. One important tool at our disposal is through the use of in vivo imaging. In fact, imaging has great potential to facilitate the translation of promising IN therapies from animals to humans and improved imaging techniques continue to emerge. Prior to discussing the imaging aspect, we will introduce the concept of IN delivery, explore the latest information regarding the most likely path from nose-to-brain and discuss various types of therapies that would benefit from IN imaging assessment. In particular, we lay the groundwork for the importance of developing theranostic agents for both therapy and diagnosis in one platform.

The nasal cavity is well-suited for therapy delivery since the nasal mucosa has a high relative permeability, thin endothelial membrane and reasonable surface area for absorption of not only small molecules but also macromolecules such as proteins and peptides, nucleotides, viruses and even stem cells [3-5]. In particular, nose-to-brain therapy delivery has garnered high interest given the high failure rate of drugs that are unable to bypass the BBB [6]. Examples of difficult-to-treat central nervous system (CNS) diseases include brain malignancies, neurodegenerative diseases, stroke, seizures and psychiatric diseases, among others [7]. Understanding the mechanism of delivery and fate of drugs that can bypass the BBB is imperative to treating these debilitating and costly diseases [8].

IN delivery offers several advantages over other routes of administration: It is relatively non-invasive, it avoids first-pass metabolism and its side effects can be minimized since other healthy organs are not exposed to the therapeutic compound [4]. Because of its non-invasive nature, there is a reduced risk of infection or disease transmission. Additionally, nasal spray formulations are easy to administer and can be performed at home by the patient. As with any route of delivery, however, there are challenges that must be overcome when using the nasal cavity for therapy delivery. Similar to the BBB, the nasal mucosal barrier poses IN delivery challenges, such as a physical boundaries provided by tight junctions, cellular membranes and enzymes in the mucosal milieu. In addition, certain environmental substances, including pathogens and allergens, can irritate the nasal mucosa and full delivery of a drug may be impaired when a patient has an active upper respiratory infection. Mucociliary clearance can also hinder the delivery of intranasally administered therapeutics. Thus, only a small percentage of the administered drug may arrive at the target site following IN delivery; so, a compound requiring relatively high concentrations for therapeutic efficacy may not be an ideal candidate for this route.

Aside from its purported role as a promising route of drug delivery, the nasal cavity normally serves important roles in respiration and smell while also providing a protective barrier against environmental insults [9]. The nasal anatomy in animals can differ widely relative to humans. For instance, the ratio of surface area to luminal volume in the nasal cavity of a rat is very different from that in humans (i.e., rat is 3350 $mm^2/cm^3$ and human is 820 $mm^2/cm^3$) [10]. The relatively larger dedication of olfactory mucosa to smell in rodents allows a particularly strong model for IN delivery, but a lower contribution of olfactory mucosa to smell in humans poses a challenge when interpreting drug efficacy results from rodent data. The anterior vestibule, the respiratory region and the olfactory region serve as three different anatomically distinct areas in the nasal cavity and only the respiratory and olfactory regions are thought to contribute to drug delivery (**Figures 1** and **2**) [9, 10].

The respiratory epithelium is the largest of the three areas, is located more anteriorly within the nasal cavity, and produces the majority of the mucus, which is an additional barrier that intranasally delivered drugs must overcome for CNS delivery [11]. Drugs that overcome mucociliary clearance and make their way across the respiratory epithelium, such as naloxone and zolmitriptan, may be absorbed into the small blood vessels within the lamina propria, where they would avoid first-pass metabolism encountered with orally delivered agents, but would then still need to cross through the BBB from the systemic circulation [12]. The lamina propria of the respiratory epithelium also contains a high surface area of branches of the trigeminal neuron which, along with a multitude of small blood vessels, that provides a significant perineuronal and perivascular pathway for therapeutics to enter the brain [4, 13-15]. For instance, Lochhead et al. used ex vivo fluorescence imaging (FLI) to show that bulk flow within the perivascular space of cerebral blood vessels contributes to the rapid central distribution of small-molecule, fluorescently labeled dextran tracers after IN administration in anesthetized adult rats [15]. Labeled macromolecules, such as interferon gamma [16], insulin-like growth factor [14], and most recently insulin [17], also demonstrated rapid uptake into the brain and cerebral spinal fluid (CSF) spaces along the trigeminal route following IN administration.

The olfactory epithelium is the most posteriorly located epithelium of the nasal cavity (**Figures**

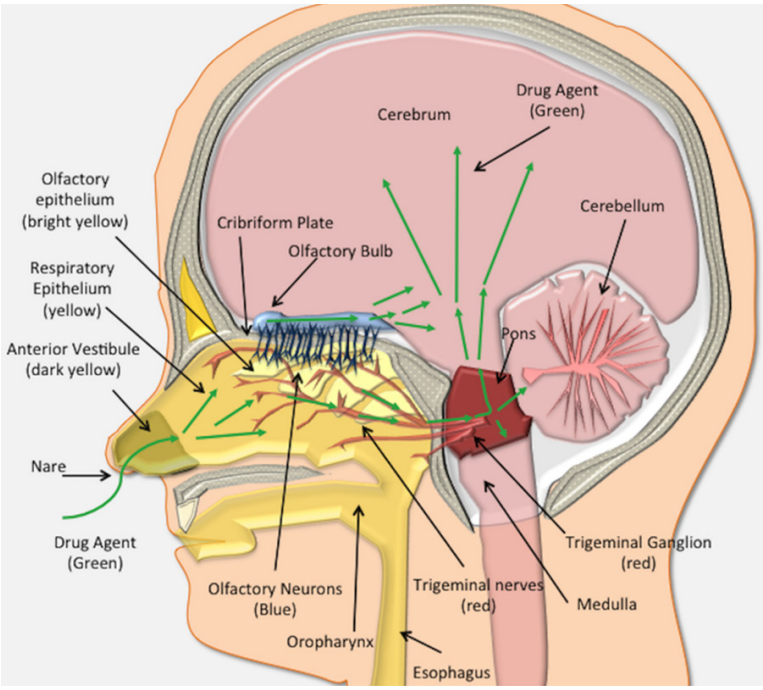


**Figure 1.** The human nose-to-brain anatomy. In humans, the nasal cavity contains three major regions based on epithelial type. The first most anterior vestibule (dark yellow), is comprised of squamous epithelial cells and does not play a significant role in drug absorption/uptake. Just posterior to the anterior vestibule is the respiratory epithelium (yellow). Drugs (green arrows) absorbed across the respiratory epithelium can be deposited into the lamina propria where they gain access to an extensive pathway to the brain along the branches of the trigeminal nerve. Drugs can travel intraneuronally or in a perineural and perivascular distribution to enter the brain via the trigeminal ganglion (red) and brainstem (red). Finally, posteriorly and dorsally lies the olfactory epithelium (bright yellow), which houses the olfactory neurons (blue), and is situated at the posterior and dorsal aspect of the nasal cavity. These neurons send cilia into the nasal cavity lumen. Drugs can be absorbed into the olfactory receptors or traverse the olfactory epithelium to gain access to the olfactory bulb by transcellular or perineuronal/perivascular routes within the lamina propria. From the olfactory bulb (blue), drugs (purple arrows) gain access to the brain (pink).

**1** and **2**), and is structurally different from the respiratory epithelium since it contains bipolar primary receptor neurons necessary for our sense of smell [18, 19]. The olfactory epithelium overlies the cribriform plate and biopsy studies of humans indicate that the olfactory region may cover more of the nasal cavity than previously thought, extending to involve the middle turbinate (**Figures 1** and **2**) [9, 20]. Like the respiratory epithelium, the olfactory neuroepithelium sits atop a highly cellular lamina propria that contains the axon fascicles as well as Bowman's glands, blood vessels, and connective tissue (**Figure 3**) [11]. However, the olfactory epithelium also contains the olfactory receptor neurons and olfactory ensheathing cells, which can serve as a means of direct intra-neuronal transport into the olfactory bulb of the brain. This direct transport is made possible if the cilia aid in cellular uptake of the therapy or provide an additional highway to the brain CSF spaces. The cilia also provide a similar highway along extensive perivascular and perineuronal spaces found with the trigeminal system within the lamina propria. The classically cited example of direct neuronal transport is wheat-germ agglutinin conjugated to horseradish peroxidase, which was visible in neuronal axons and the olfactory bulb following IN delivery in mouse, rat and squirrel monkey [21]. However, intraneuronal transport is slow with studies indicating brain entry via the olfactory nerve taking 1.5-6 hours and even longer via the trigeminal nerve, taking from 17-56 hours [3]. Since several studies have confirmed rapid nose-to-brain delivery within minutes, the intra-neuronal pathway is probably not the primary route.

*Intranasal therapies*

The various IN therapies that have been attempted and published are extensive. The current review provides only examples to give a flavor of intranasally delivered therapies. For a more detailed description specific to therapies, the reader is referred to the following reviews by Fortuna et al. [22], Erdő et al. [23] and Corrigan et al. [24]. Although more often for systemic or local treatment, examples of therapies currently used clinically through the IN route include nasal sprays for allergic rhinitis (Azelastin Hydrochloride: Astelin, Meda Pharmaceuticals, Inc.), the common cold (Oxymetazoline: Afrin, Merck and Co, Inc), vaccines

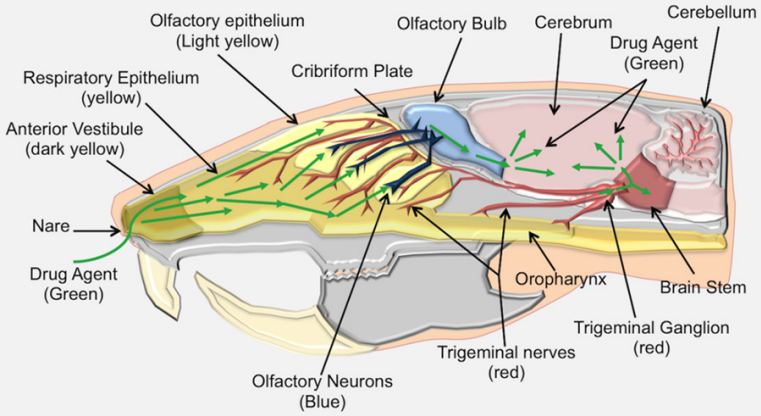


**Figure 2.** Rat nose-to-brain anatomy. The nose-to-brain anatomy of the rat is similar to the human with a few differences. Compared to the human, the rat nasal cavity has a relatively greater surface area in the olfactory system, making it an ideal animal model for studying IN delivery. The rat nasal cavity consists of the anterior vestibule (dark yellow), respiratory epithelium (yellow), transitional epithelium and olfactory epithelium. Drugs (green arrows) gain access to the brain along the olfactory and trigeminal pathways, similar to human IN delivery.

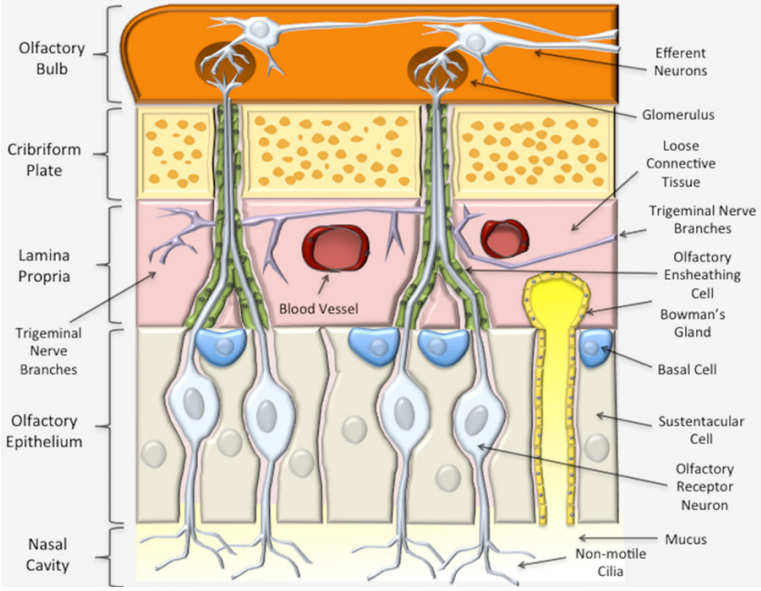


**Figure 3.** Olfactory nasal mucosa. The olfactory epithelium is mostly comprised of olfactory receptor cells and sustentacular support cells. Deep to the olfactory epithelium is the lamina propria (pink), which contains blood vessels, lymphatics and abundant branches of the trigeminal sensory neurons. Compounds deposited into the lamina propria can travel in a perineural, perivascular or perilymphatic manner to access the brain (orange). The axons of the olfactory cells traverse the lamina propria and form nerve fascicles, called the fila olfactoria. Olfactory ensheathing cells (green) pass through the cribriform plate (yellow) along with the olfactory nerve axons. The olfactory neuron axons synapse in olfactory bulb with second order neurons that then travel to other parts of the brain.

(FluMist Quadrivalent, MedImmune, LLC), and others. Agents currently undergoing clinical trials, many of which take advantage of the nose-to-brain route, include IN insulin for memory (NCT02758691), post-traumatic stress disorder (PTSD) (NCT04044534), mood disorders [25], and Alzheimer's disease [26, 27]; IN glutathione for Parkinson's disease (NCT01398748) [28]; IN oxytocin for autistic spectrum disorder [29, 30], Prader-Willi syndrome [31], attention-deficit/hyperactivity disorder (ADHD) [32] dementia [33], and schizophrenia; IN dexmedetomidine for sedation of patients with autism spectrum disorder (NCT03597477); IN fentanyl for cancer pain management (NCT00994760); nerve growth factors for stroke (NCT03686163) and IN neuropeptide Y for PTSD (NCT01533519) [34]. Clinical trials of IN delivery are often focused in pediatrics because of the relatively greater ease of IN administration compared to intravenous (IV) delivery and better patient comfort for pediatric patients. These include dexmedetomidine for IN anesthesia (NCT03597477), IN ketorolac for pain (NCT02297906), and midazolam for anti-anxiety (NCT03635398). In addition to clinically approved drugs, the number of compounds undergoing experimental evaluation using the IN route in animal models is extensive and beyond the scope of this review.

Therapeutic compounds delivered intranasally vary widely and each type of therapy has important challenges to consider. In this review, we delineate small molecules which are less than 900 Daltons from macromolecular compounds, such as nucleic acids and peptides/proteins. We also discuss two additional cate-

gories: Nanosystems, including nanoemulsions (NEs) and nanoparticles (NPs), as well as therapeutic stem cells [35]. While all of these categories could be adapted to serve as theranostic agents, nanosystems and cellular therapies are particularly suited for this emerging concept, which combines therapy with diagnostic information. Typically, nanosystems and cells have the greatest potential to adapt to become theranostic agents. It should be noted, however, that not every theranostic agent is in the form of a nanosystem.

*Small molecules*

Small-molecule drugs are among the most common intranasally delivered therapies administered to humans because of their small size (less than 900 Da), which allows for rapid diffusion across cell membranes. Examples of clinically approved small molecules include anesthetic agents [36] as well as drugs that treat migraines [37], treatment-resistant depression [38], seizures [39], pain modulation [40, 41] and antidotes for drug overdose (i.e., naloxone) [42]. More experimental examples at the preclinical level include morphine and oxycodone for the reduction of intentional drug abuse [43, 44] and doxylamine in subjects with sleep impairment [45]. Since many small molecules are already approved for human use via topical, enteric or IV routes of administration, the regulatory burden for approval of IN delivery of small molecules is small [22]. However, most small molecules that can be used intranasally can also be delivered orally. In addition, many of the above-listed small molecules may utilize the nose-to-brain route to some extent, but the majority is likely to become systemically available following absorption across the nasal membrane barrier [46].

Nose-to-brain delivery of drugs occurs through a variety of different pathways; therefore, to optimize a small molecule for maximum delivery, it is important to tailor the molecule to travel through any of the possible pathways rather than focus on any one [47]. Designing the best small molecule would involve balancing a variety of factors including hydrophilicity, polarity, charge, size and molecular interactions. Mucin, which is a glycoprotein constituent of mucus, has both hydrophobic and hydrophilic components. While hydrophilic drugs are very soluble in mucus, leading to high clearance, extremely hydrophobic agents may interact with the mucus and fail to reach the nasal cavity [3, 22]. To achieve the highest probability of transport, a drug needs to exhibit moderate hydrophilic properties to minimize hydrophobic interactions with the mucus and maintain the ability to be dissolved in aqueous medium, all while avoiding clearance. Molecules that are polar tend to have low bioavailability since they are prone to clearance or decomposition by nasal enzymes [22]. In terms of charge, mucin is negatively charged; so, to minimize electrostatic interactions that would cause drug entrapment within the mucous, the drug needs to be neutral or slightly negative at physiological pH [3]. While small molecules are generally not inhibited via size restraints, it is necessary to design these molecules in a way that limits potential molecular interactions that would trap them in the nasal mucosa for clearance and prevent absorption across the mucosa [48].

*Macromolecular agents*

IN delivery provides a viable route to the CNS for macromolecular agents if they can overcome the anatomic and functional impediments of the nasal mucosal barrier. Examples of macromolecular agents include most drugs that are larger than 900 Da by molecular weight, but more specifically include agents that are not likely to be absorbed following oral delivery such as peptides, proteins, and nucleic acids. These agents are commonly called biologics, which are considered a collection of macromolecular compounds with a high potential for therapy. Most proteins [22] and even therapeutic plasmids [49] and viruses [50] would fall into this category. Therapeutic neuropeptides belong to a class of small peptides. They are promising for IN drug delivery for CNS applications because of their decreased molecular weight compared to larger proteins and macromolecular compounds. A good example in this group is oxytocin, which has been studied extensively as a psycho-modulator of several cognitive responses and social interactions [51, 52] and has been used in clinical trials to treat mental disorders [53-55].

Macromolecules are prone to the same issues as small molecules since these, too, must traverse the aforementioned barriers and abide

by optimization guidelines. Compared to small molecules, macromolecular agents are much more sensitive to size and, as the molecular weight increases, the absorption rate decreases [48]. Given the limitations encountered with delivering small molecules and macromolecules across the nose-to-brain barriers, several absorption-enhancing materials are being investigated and developed, including cell-penetrating peptides (i.e., penetratin [56, 57]), agents that open the tight junctions between cells (i.e., chloramphenicol acetyltransferase and matrix metalloproteinases [58]), and even agents that reversibly destroy the most superficial layer of the nasal mucosa (i.e., methimazole [59]). However, with the implementation of enhancers, there is a risk of a leaky BBB and a risk of CNS infection, potentially leading to brain edema [3]. In addition, macromolecules are subject to other challenges such as higher susceptibility to enzymatic degradation, from lower permeability and shape restraints [22]. Furthermore, it was found that linear molecules seem to have lower absorption than cyclic molecules [22]. The optimization of small and large molecules was outlined by Kumar et al. [48]. Some characteristics to look for include therapeutic effects at lower volumes, appropriate nasal absorptive characteristics, minimal nasal irritation, higher drug stability, and minimized odors or other comfort deterrents with the therapy [48].

*Nanosystems*

Despite the potential advantages of IN delivery to circumvent the BBB, most small-molecule and macromolecule therapies in solution must still overcome several obstacles in transit to the brain or CSF spaces. It is estimated that 98% of low-molecular-weight molecules and 100% of high-molecular-weight macromolecules fail in entering the CNS due to physiological and physiochemical challenges [48, 60]. The extremely low bioavailability of these molecules challenges their use intranasally. However, concentration levels can be further manipulated by nanotechnology-based systems, nanosystems. Specific examples that can be grouped more broadly into nanosystems would include nanogels, dendrimers, nanosuspensions, NEs, and NPs, to name a few [48, 61]. Drug-loaded nanosystems present various advantages that have potential to overcome the aforementioned challenges. These include improved endothelial permeability and extravasation, enhanced interstitial diffusion and decreased clearance or trapping by phagocytes. Additionally, nanosystems can be decorated with disease-specific ligands that target biomarkers of interest, thereby improving their biodistribution profile and minimizing toxicity to healthy tissues. Incorporating CNS drugs into nanosystems can also preserve the pharmacological action and physicochemical integrity of the drugs and reduce their dilution with body fluids. These advantages can significantly improve the safety profiles of CNS drugs and increase their maximum tolerated doses (MTDs). Overall, to justify an agent's delivery via a nanosystem, its incorporation must overcome the limitations associated with free drug. Furthermore, drugs that are quickly cleared need to have increased absorption and the nanosystem must protect the drug from enzymatic degradation in the nasal cavity. Strong drug candidates would include low water solubility, instability, slow onset of action, and those requiring high dosages that create systemic side effects [60]. Optimal nanosystems would remain less than 200 nm as the diameter of olfactory axons ranges from 100 nm to 700 nm and the mesh size of mucin ranges from 20 nm to 200 nm [3, 60]. To sum up, the benefit of using a nanosystem as a drug carrier and/or solubilizer is the ability to modify and fill in any weaknesses associated with the delivery of free drugs. There are a variety of different materials available to complete this.

Further optimization methods address the challenges discussed above. Each nanosystem has distinct advantages, but NPs and NEs will be described in brief specifically, outlining their role in IN delivery and imaging. For a more detailed information regarding nanosystems, the reader is referred to reviews from Kumar et al. [48], Patra et al. [62], and Chavda [61].

NPs are compact particles with diameters ranging from 1 to 1000 nm [48]. They can be fabricated by a variety of procedures including solvent evaporation, ionic gelation, or precipitation [61, 63]. NPs may be composed of biodegradable and non-biodegradable constituents and can be categorized as polymeric, polymeric micelles, liposomal, and inorganic, among others [64]. Polymeric NPs are often the

simplest type, utilizing single polymer chains. Alteration of polymer molecular weights allows fine tuning of drug release kinetics. Polymeric NPs can be fabricated with a variety of different methods including dispersion of polymers, polymerization of monomers, and ionic gelation [65]. Polymeric micelles are self-assembled polymeric amphiphiles that can deliver hydrophobic drugs, though there have been studies utilizing them to deliver hydrophilic imaging agents which were loaded into micelle's core through polymer-metal complex formation [66]. Liposomal NPs are also self-assembled via methods such as nanoprecipitation [67], thin-film hydration and extrusion [68], and electrospinning [69] and can encapsulate both hydrophobic and hydrophilic drugs and imaging agents. Finally, inorganic NPs offer advantages for both imaging and therapy as they contain materials such as iron oxide, gold and silica, among others. Gold NPs, in particular, are useful as they have also been studied as radiosensitizers for cancer cells [70]. These are non-biodegradable and are very small, less than 100 nm. Several NPs are FDA approved for human use and are extensively outlined by Bobo et al. including polymeric NPs (Copaxone® and Eligard®), polymeric micelles (Estrasorb™), polymer-protein conjugates (e.g., PegIntron®, Somavert), liposomal NPs (Marqibo®, Doxil®/Caelyx® and Onivyde®), and inorganic NPs (Nanotherm®, Ferrlecit®, and Feraheme™) [64]. One example of current research is polycaprolactone polymer NPs prepared by nanoprecipitation. They are being investigated for the nose-to-brain delivery of melatonin for the treatment of glioblastoma. Compared to free drug, melatonin NPs had significantly improved therapeutic efficacy, reducing the amount of drug required [63]. Bioavailability of NPs has been a debatable subject as IN delivery poses the same physical and chemical barriers like other drugs; the difference is that NPs offer more chances to finely tune the delivery system [48]. Furthermore, there are general challenges such as macrophage recognition of surface moieties. A variety of mucoadhesive polymers are incorporated to extend adhesion time in the nasal cavity, thereby preventing clearance. These include chitosan, alginates and cellulose [22]. Increased adhesion time as a mean to promote increased therapy remains controversial. On one side, increased adhesion prevents transport to the brain. On the other, increased adhesion prevents clearance and increases the chance of endocytosis [3]. Other challenges include premature release of drugs, toxicity and achieving desired dose requirements [61].

NEs are nano-sized globules that are biphasic, containing two immiscible liquids (water/oil) and a variety of surfactants and co-surfactants [71]. Some commercially available NEs, not specific to nose-to-brain delivery, include Diazemuls®, Lipuroetomidate® and Diprivan®, etc. Unlike NPs, there is no distinct boundary of each droplet; however, the globule is typically known to have sizes of 100-300 nm or less [60]. NEs are either oil-in-water (O/W) or water-in-oil (W/O) emulsions fabricated by high energy (ultrasonication/homogenization) or low energy (phase inversion by temperature/composition changes) techniques [60]. However, to our knowledge, only an O/W emulsion is used for IN administration of drugs. NEs interact directly with the aqueous environment via Brownian motion of the droplets [48]. NEs, like NPs, allow the transport of hydrophobic drugs into the brain. For example, saquinavir is an anti-HIV drug, but its water insolubility renders it a strong candidate for delivery via a NE. NEs showed an increase in permeation into the brain compared to free drug [60]. Another study by Colombo et al. analyzed the effects of incorporating chitosan into NEs [72]. Chitosan is heralded in NEs for its ability to act as a mucoadhesive to decrease nasal clearance [71]. A NE containing kaempferol was made with and without conjugation to chitosan for the treatment of glioma. It was found, in an ex vivo analysis, that NEs conjugated to chitosan significantly increased permeation across the mucosa because of the electrostatic interaction of positively charged chitosan and negatively charged mucosal layers, while also significantly increasing the amount of drug delivered to the brain [72]. Mucoadhesives appear to be quite critical in avoiding NE clearance and their use optimizes drug delivery [71]. Uniquely, NEs use a high concentration of surfactants that can be chosen from a list of generally regarded as safe (GRAS) agents including polyethylene glycol (PEG) 8 stearate, PEG 400, polysorbate 20 and propylene glycol, to name a few [61, 71]. Such surfactants can provide a fluidizing effect on the barrier endothelial cells, promoting drug permeability within the olfacto-

ry and trigeminal pathways [60]. Despite their advantages, those surfactants need to be monitored for toxicity with repeat dosages. Furthermore, both NPs and NEs are subjected to scale-up challenges. In a laboratory setting, these systems are made using specific material amounts in a specific order, which makes their translatability to industry a challenge.

*Cellular therapies*

IN delivery of stem cells to the brain overcomes the certain challenges associated with brain drug delivery and is highly amenable to theranostics. Multiple studies have confirmed the localization of various stem cells in the brain following IN delivery, including mesenchymal stem cells (MSCs), neural stem cells (NSCs) and pluripotent stem cells [73, 74]. MSCs were delivered to the brain via the IN route, successfully treating animal models of neurodegenerative diseases, including Parkinson's disease, Alzheimer's disease and Huntington's disease [75-77]. MSCs have also been delivered intranasally for the treatment of stroke [78, 79], including neonatal hypoxia-ischemia [80, 81]. In addition, MSCs delivered via nasal application imparted therapeutic efficacy when expressing tumor necrosis factor (TNF)-related, apoptosis-inducing ligand in a mouse model of human glioma. The increased overall survival was even higher when the mice had been irradiated [82]. The irradiated mice showed higher levels of CXCL12, a lymphatic chemokine, which is possibly related to the mechanism of migration of those cells [83]. Although radiotherapy is a highly effective tool for the treatment of brain cancer, it also causes detrimental effects in surrounding healthy tissues, leading to pernicious neurocognitive side effects. A novel strategy to mitigate the negative effects of radiation in brain tumor treatment involved IN administration of human MSCs, which promoted brain injury repair and improved neurological function following brain irradiation in mice [84]. Stem cells have become carriers of oncolytic agents or drugs due to their capability to target brain tumors when the stem cells and tumor cells express specific cell adhesion molecules. For instance, CXCR4-enhanced NSCs delivered an oncolytic virus to glioma and extended survival of animals when they received concomitant radiotherapy [85]. Moreover, neural stem/progenitor cells (NSPCs) displayed a rapid, targeted tumor tropism with significant accumulation at the intracranial glioma site within 6 hours after IN delivery. This peaked at 24 hours and remained at this level for up to five days. Currently, two clinical trials are assessing IN delivery of stem cells in the brain. One is recruiting to evaluate the use of autologous bone marrow-derived stem cells (BMSC) to improve cognitive function (NCT03724136). Another is also recruiting to study the use of autologous BMSC and its transfer to the vascular system and inferior 1/3 of the nasal passages in order to determine if such treatment will provide improvement in neurologic function for patients with a broad spectrum of neurologic conditions (NCT02795052). Overall, cellular therapies are an emerging therapy that may offer many benefits for IN delivery.

*Theranostics*

The development of a single platform for the simultaneous delivery of therapeutics and diagnostic imaging agents for pretreatment planning, real-time tracking/monitoring and/or posttreatment assessment provides the basis for the emerging field of theranostics [86]. Molecules such as metaiodobenzylguanidine (MIBG) containing iodine-131 ($^{131}$I) and iodine-123 ($^{123}$I), somatostatin peptide analogs labelled with lutetium-177 ($^{177}$Lu) and prostate-specific membrane antigen (PSMA) labelled with $^{123}$I, $^{131}$I, gallium-68 ($^{68}$Ga), $^{177}$Lu and yttrium-90 ($^{90}$Y) have been used as theranostic materials in nuclear medicine [87, 88]. Also, radioactive $^{131}$I is used to simultaneously image and treat thyroid diseases [89]. In general, direct imaging of small-molecule and macromolecular therapies following IN delivery in vivo is difficult to do since the addition of an imaging tracer runs the risk of interfering with drug binding site, thereby altering therapeutic efficacy. Imaging labels directly conjugated onto the therapeutic agent may also negatively alter biodistribution and pharmacodynamic/pharmacokinetic profiles. Regardless, direct labeling of drugs would benefit from in vivo imaging to better understand the ultimate fate of therapies after delivery, which includes the route of transit from nose-to-brain. When developing therapies that utilize nanosystems or cells, labeling agents for in vivo imaging becomes more feasible, albeit still technically

challenging. A recent NP-based drug delivery system was formulated for the treatment of glioblastoma by Sukumar et al.; it provides a comprehensive example of the multiple functions NPs can have. Briefly, gold-iron oxide NPs loaded with microRNAs for IN delivery were produced to provide a multi-functional theranostic capability for the treatment of glioblastoma. These NPs were coated with β-cyclodextrin-chitosan (CD-CS) hybrid polymer for the co-loading of the microRNAs. Finally, the NPs were decorated with PEG-T7 peptides to specifically target glioblastoma cells. In vivo analysis showed that these multi-functional NPs provided tumor sensitization, via the microRNAs, to the standard-of-care treatment, temozolomide, improving overall survival. Because of the gold-iron oxide component, the IN delivery of the NPs was monitored via $T_2$-weighted magnetic resonance imaging (MRI) [90].

*Intranasal imaging*

In humans, IN imaging studies have thus far been limited mostly to MRI, positron emission tomography (PET) and single-photon emission computed tomography (SPECT), with MRI being the most extensively utilized modality. Gamma scintigraphy, to our knowledge, has been used clinically in the context of IN imaging in one instance. Preclinical studies that utilize imaging offer a great deal of information about the fate of the delivered therapeutic and/or disease progression, which would enable the efficacy of novel IN therapies and their potential for clinical translation. So far, preclinical imaging studies have not only utilized MRI, PET and SPECT but also gamma scintigraphy as well as bioluminescence imaging (BLI) and fluorescence imaging (FLI). Ultrasound imaging, however, has not yet been used for IN imaging by virtue of the difficulties associated with transmitting and receiving acoustic waves across osseous structures using diagnostic ultrasound transducers in the clinical megahertz ranges. Nevertheless, ultrasound waves can be focused using specialized therapeutic focused transducers in order to enhance transmission and enable therapeutic benefits for IN drug delivery; this emerging approach, which is known as focused ultrasound-mediated drug delivery, will be briefly discussed later in this Review. A few CT studies have been used in humans and animals, mostly to study nasal anatomy and nasal flow dynamics. Combined PET and MR has perhaps the highest future potential for the assessment of the nose-to-brain route of drug delivery since they can combine both the high quantitation and sensitivity of molecular imaging with the high tissue contrast and spatial resolution of MRI. However, very few studies have been performed to date using this dual-modality approach which enables understanding of in vivo biological processes at a fundamental level. In subsequent paragraphs, we review each imaging modality and its contribution to understanding IN delivery from both a preclinical and clinical perspective.

*Magnetic resonance imaging*

MRI is a powerful, non-ionizing imaging technology that utilizes a strong magnet (typically 0.5-3 tesla for humans and up to 21.1 tesla for small animals) to produce three-dimensional detailed anatomical images [91]. MRI has revolutionized medicine because of its ability to generate high spatial resolution images and exquisite soft tissue contrast (**Table 1**). In humans, it is used for disease detection and therapy monitoring. MRI signals are produced through the process of resonance using radiofrequency (RF) coils, which include a transmitter and receiver. The RF transmitter coils generate a secondary magnetic field ($B_1$) that is perpendicular to the main magnetic field ($B_0$), whereas the RF receiver coils detect the resulting MR signal. The transmitter and receiver functions are often separated in order to maximize the signal-to-noise ratio (SNR) of a given imaging sequence [92]. Image contrast in MRI is mainly based on inherent properties of biologic tissues; these include proton content (i.e., $^1$H spin density), longitudinal recovery time ($T_1$) as well as transverse relaxation times ($T_2$ and $T_2^*$) of $^1$H nuclei [93, 94]. MRI of the brain allows a high level of detail and with the use of higher magnetic fields, animals as small as mice can be imaged. Although MRI is widely available clinically, only certain centers of research have more sophisticated MRI capability at the small-animal, preclinical level. Multimodality, multiparametric imaging in small animals is even less frequently available. Regardless, these technologies are continuously evolving to reduce the costs and scan times as well as improve

**Table 1.** Comparison of imaging modalities utilized in intranasal delivery of therapeutics to the brain

| Imaging modality | Strength | Weakness | Spatial resolution | Sensitivity |
|---|---|---|---|---|
| MRI | -No ionizing radiation<br>-Excellent soft-tissue contrast<br>-Superior spatial resolution with multiplanar imaging capabilities<br>-Very versatile and widely available for both preclinical and human imaging studies<br>-Can utilize magnetofection | -Expensive<br>-Gd-based contrast agents can be toxic<br>-Susceptible to patient movement-induced image artifacts<br>-Relatively slow patient throughput<br>-Some patients may experience claustrophobia<br>-Safety hazards for patients with implanted medical devices<br>-Possible thermal injuries in the body and hearing issues | +++++ | ++ |
| CT | -Provides detailed images of many tissue types, including osseous tissue<br>-Can image soft tissue, bone and blood vessels simultaneously<br>-Relatively inexpensive and fast compared to MRI<br>-Unlike MRI, patients with implanted medical devices are safe inside a CT scanner<br>-CT is less sensitive to patient motion than MRI<br>-Can complement PET or SPECT, both clinically and preclinically<br>-Micro-CT is available for laboratory use | -Involves ionizing radiation<br>-Patients may experience adverse reactions to contrast agents<br>-Generally, not recommended for pregnant women | ++++ | + |
| Gamma Scintigraphy | -Easy to use, fast and inexpensive<br>-Provides functional information<br>-Can be used in drug discovery and development to facilitate pharmacokinetic/pharmaco-dynamic and biodistribution studies<br>-Higher spatial resolution than SPECT | -Involves ionizing radiation<br>-2D images with poor spatial resolution compared to MRI or CT<br>-no CT or MR combination for anatomy overlay<br>-Lower detection sensitivity compared to SPECT<br>-Requires physical collimators that reject photons that are not within a very limited angular range, thereby decreasing sensitivity compared to PET | +++ | ++ |
| SPECT | -Enables noninvasive visualization of biodistribution of radiolabeled tracers for diagnostic applications and assessment of treatment efficacy<br>-Utilizes common radiopharmaceuticals, like Tc-99m, that are widely available<br>-Relatively inexpensive -Can be employed in a dual-modality system (SPECT/CT)<br>-Can do multi-isotope imaging (i.e., multi-radioisotope resolution)<br>-Can allow for widening observational time window of imaging due to the longer half-life of single photon emitters | -Involves ionizing radiation<br>-Less quantitative than PET<br>-Requires collimation which introduces noise, decreases sensitivity, and increases san time<br>-Relatively poor spatial resolution compared to MRI or CT | ++ | +++ |
| PET | -More sensitive than SPECT (two to three orders of magnitude)<br>-Many radiopharmaceuticals are available<br>-Short-lived radionuclides used in PET improve detection sensitivity<br>-Quantitatively accurate<br>-Most often as a molecular imaging modality combined with CT and most recently with MRI<br>-Micro-PET is available for animal studies | -Involves ionizing radiation<br>-Expensive<br>-Requires complex equipment<br>-Quantitative data analysis depends on specialized software tools<br>-Relatively poor spatial resolution compared to MRI or CT | ++ | +++++ |
| Optical | -Safe, sensitive, widely available, inexpensive with high spatial resolution<br>-Nonionizing radiation<br>-Fast (e.g., multiple animals can be imaged at once, reducing imaging operation time and costs)<br>-Can be used to monitor disease progression, therapeutic efficacy and molecular processes | -Unusable for deep tissues<br>-Cannot be performed non-invasively in vivo on brain easily secondary to skill | ++++++ | ++++++ |

software interfaces for the use of MRI in both the clinical realm and the investigational setting in both humans and animals.

Contrast agents utilized in MRI include gadolinium-based contrast agents (e.g., gadolinium-diethylenetriamine pentaacetic acid (Gd-DTPA)) and iron-containing agents. Gadolinium-based agents allow for contrast enhancement and image brightening by shortening $T_1$ times of hydrogen nuclei in contrast agent-containing biologic tissues, further delineating regions of interest (e.g., tumors). Iron, on the other hand, is visualized using $T_2$- or $T_2^*$-weighted MRI parameters by shortening $T_2$ times and inducing a hypointense signal. Moreover, by utilizing fluid- or fat-eliminating techniques (e.g., FLAIR, STIR, and T2 fat saturation), the pathology can often be better visualized. Certain sequences, including gradient recalled echo (GRE) and susceptibility-weighted imaging (SWI), detect hemorrhage or calcification through what is known as a blooming artifact. In addition to static imaging, MRI can be used to collect dynamic information such as with various perfusion techniques, which are more commonly utilized in stroke and tumor imaging. Examples of perfusion techniques include dynamic susceptibility contrast, dynamic contrast enhancement and arterial spin labeling. Another MRI technique that can detect the diffusion of water through space is known as diffusion-weighted imaging (DWI). DWI is the clinical workhorse for the detection of stroke and abscesses. Diffusion tensor imaging (DTI) is another diffusion-related sequence which analyses the three-dimensional shape of the diffusion of water in space to generate an image. Similarly, functional MRI (fMRI) indirectly measures oxygen utilization in certain resting states or activated brain regions to generate regional maps of brain activity.

In animals, MRI can be performed at baseline and following therapy to assess changes in the brain compared with the original baseline. Examples include animal models of brain tumors such as glioblastoma [59, 74, 83], stroke [95] autistic spectrum disorder [96], multiple sclerosis [97], and neuroinflammation [98]. Using DTI and metric fractional anisotropy, IN delivery of myelin oligodendrocyte glycoprotein ($MOG_{35-55}$) was shown to ameliorate progression of disease and reduce brain damage in a mouse model of multiple sclerosis [97]. The neuroprotective peptide, NAP (part of the 8 amino acids in NAPVSIPQ) also called davunetide (CP201), which is derived from activity-dependent neuroprotective protein (ADNP) was pioneered by Dr. Gozes and her team. This promising agent has been shown to be neuroprotective in numerous neurodegenerative animal models of disease, including Alzheimer's disease, Parkinson's disease, frontotemporal dementia and amyotrophic lateral sclerosis [96]. Most recently, the group demonstrated the neuroprotective effects of NAP augmented by the penetration enhancer chorabutanol in ADNP+/- mouse model of autistic-like ADNP syndrome. Using a 7-tesla MRI unit for in vivo imaging of seven eight-month-old mice, NAP protected against abnormal increases in DTI-derived mean diffusion and fractional anisotropy in the hippocampus in the ADNP+/- mice following IN delivery of NAP, demonstrating its translatability to clinical practice. In an interesting study, Zhang et al. utilized DTI-derived fractional anisotropy and other histologic techniques to demonstrate a regenerative role of interleukin-4 (IL-4) beyond its known immunoregulatory functions in an experimentally induced middle cerebral artery occlusion mouse model [95]. IL-4-loaded liposomal NPs were administered intranasally at 1-7 days, 14 days, 21 days and 28 days following middle cerebral artery (MCA) occlusion and was found, using in vivo DTI on a 9.4-tesla MRI system and histologically, to improve white matter integrity. Long-term sensorimotor and cognitive deficits also improved in the IL-4 NP-treated group compared with vehicle-treated mice.

Direct localization of therapeutic agents in MRI have so far been limited to nanosystems and cellular therapies. For instance, a cholera toxin B subunit-derived NP was found in the hippocampus at one hour after IN delivery in a mouse [99]. By tagging the cholera B toxin NPs with Cy5.5 (an internal fluorescence probe that served as a model drug) and $Gd^{3+}$ (an MRI contrast agent), 7-tesla MR images were obtained in vivo followed by ex vivo histologic and fluorescence microscopy of brain sections. Although the authors claimed that the cholera toxin could be a nanosystem for the treatment of Alzheimer's disease and could target the hippocampus, a therapeutic drug was not delivered and a mouse model of Alzheimer's dis-

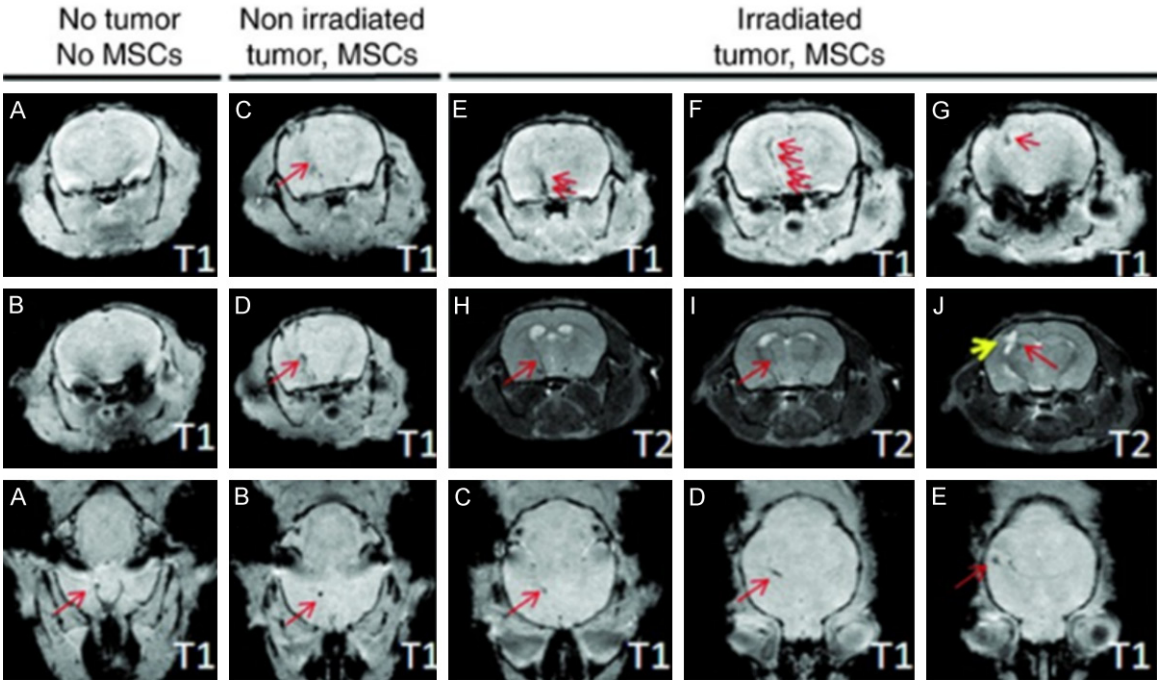


**Figure 4.** High-resolution $T_1$- and $T_2$-weighted MRI of intranasally administered MSCs. (Adapted from Balyasnikova et al., 2014 with permission). High-resolution $T_1$- and $T_2$-weighted MRI of intranasally delivered MSCs, loaded with MPIOs, were visualized migrating to the brain of irradiated intracranial glioblastoma-bearing mice to a greater degree than non-irradiated glioblastoma-bearing mice. Top two rows are in the coronal plane and bottom row is an axial plane. Red arrows point to dark signal representing the MPIOs.

ease was not utilized in this study [99]. In another study, MRI was utilized by Balyasnikova et al., to demonstrate the localization of MSCs to the tumor site in an animal model of glioblastoma at 48 hours following IN delivery [83]. The MSCs were engineered to express TNF-related apoptosis-inducing ligand (TRAIL) on the cell membrane for improved therapeutic efficacy in an irradiated glioblastoma mouse model. Additionally, the MSCs were loaded with micron-sized paramagnetic iron oxides (MPIOs) and then delivered intranasally to the brains of irradiated and non-irradiated mice with glioblastoma. The mice were then imaged 48 hours later with MRI utilizing a high-resolution, $T_2$-weighted rapid acquisition with relaxation enhancement (RARE) spin-echo images and multi-slice, high-resolution, $T_1$-weighted, fast low-angle shot (FLASH) gradient-echo sequences (**Figure 4**). Importantly, the authors utilized a clinically relevant imaging modality for the first time to demonstrate delivery of MSCs to the brain from the nose. More recently, Spencer et al. intranasally administered NSCs loaded with superparamagnetic iron oxide nanoparticles (SPIONS) with methimazole to a mouse model of glioblastoma [59]. The mice were imaged at 24 hours, 48 hours, and 120 hours following NSC treatment using a 7-tesla Bruker MR scanner. The pre-treatment addition of methimazole delayed mucociliary clearance of the NSCs from the nasal cavity for 24 hours and amplified localization to the tumor site to a greater extent than without a pre-treatment methimazole administration. Another study demonstrated IN delivery of insulin in a rat model of moderate traumatic brain injury (TBI) by MRI, performed at days 3 and 9 post injury, to result in a significant decrease in hippocampus lesion volume [100]. $^{18}$F-fluorodeoxyglucose ($^{18}$F-FDG) PET imaging was also performed on days 2 and 10 to demonstrate reduced inflammation and decreased cerebral glucose uptake, which are additional attestations to the therapeutic efficacy of insulin in TBI following IN delivery in this same animal model.

Furthermore, IN delivery of the anti-inflammatory and neuroprotective agent cyclosporine-A, contained within an oil-based, omega-3 fatty acid-rich flaxseed NE system, demonstrated therapeutic efficacy by inhibiting proinflamma-

tory cytokines in lipopolysaccharide-induced rat model of neuroinflammation as compared to a similar solution formulation without NE [98]. The $T_1$ MRI contrast agent gadolinium was complexed with the same NE system in place of cyclosporine-A. Using a 7-tesla MRI unit, the authors showed a higher uptake of the NE-gadolinium conjugate in major regions of the brain when dosed intranasally based on changes in $T_1$ relaxation times. Since cyclosprin-A does not appear to also have been included in the MR-imaged preparation, the results can only be used to indirectly imply that the cyclosprin-A also reached this location in the brain.

A novel theranostic application is to utilize the high magnetic force of MRI to guide magnetic therapeutic agents to the desired location in the brain, a term that has been described as magnetic transfection or magnetofection. For instance, in a mouse model of TBI, chitosan- and polyethyleneimine-coated magnetic micelles were evaluated as a potential MRI contrast agent using a reporter DNA delivered to the brain after mild TBI [101]. Magnetofection was also used to increase the concentration of the chitosan- and polyethyleneimine-coated magnetic micelles in the brain, suggesting the possibility of using these as theranostic delivery vehicles.

With regards to human imaging of IN delivery, a multitude of recent articles have been published to demonstrate the effects of insulin and oxytocin on various CNS conditions (for a recent review of insulin, see Santiago and Hallschmid, 2019 [102] and for recent reviews of oxytocin, see Ding et al. [103], De Cagna et al. [104], and Horta et al. [105]). IN insulin is predominately being studied as a modulator of metabolic control (i.e., obesity and diabetes) and memory (i.e., mild cognitive impairment and Alzheimer's disease) [102]. Oxytocin, on the other hand, is being studied in categories that include stress and anxiety, metabolism and weight, social engagement and bonding and pain and inflammation [105]. In a study examining the effects of insulin on memory in Alzheimer's patients, 3D MRI volumetry using 3D $T_1$ volumetric magnetization prepared rapid gradient echo (MPRAGE) sequences correlated with improved cognition and daily function following IN delivery of insulin [106]. In particular, for patients who experienced improvement in their memory following IN delivery subregional brain MRI volumes of the middle cingulum, cuneus, hippocampus, superior frontal, and parietal regions, were higher in Alzheimer's patients compared with normal patients. In another study, arterial spin labeling MRI perfusion was utilized to measure central insulin action in the brain following IN delivery in lean, overweight, and obese adults to identify brain regions affected by insulin resistance. Insulin action was selectively impaired in the prefrontal cortex in 23 overweight and obese adults compared to 25 healthy control patients, potentially by promoting an altered homeostatic set point and reduced inhibitory control contributing to an over-eating behavior [107].

Since insulin is one of the most extensively studied agents in clinical trials following IN delivery, an fMRI study was performed to assess three commercially available insulin nasal delivery devices [108]. fMRI revealed a significant decrease in regional blood flow in areas dense in insulin receptors in the intranasally delivered insulin group compared to saline alone. Also, using fMRI, oxytocin (24 IU) or placebo was delivered intranasally to 15 healthy patients in a randomized, double-blind manner to affect the precuneus and amygdala, key brain regions in social cognition and introspective processing [109]. In the nasal oxytocin study, fMRI measuring amygdala activity showed that body dysmorphic patients had higher baseline resting state functional connectivity compared to placebo, which was reversed by oxytocin IN delivery. fMRI identified highly detailed and specifically localized areas of functional connectivity between brain regions [110]. In a separate study in humans, perillyl alcohol was delivered intranasally for the treatment of glioblastoma and lower grade gliomas in patients also receiving surgery, radiotherapy, and chemotherapy. Perillyl alcohol was found to be safe and demonstrated anti-tumor activity as assessed by MRI and CT after six months of treatment [111].

*Positron emission tomography*

PET is a promising, highly quantitative and sensitive imaging tool used in disease diagnosis as well as the prediction and assessment of therapy response [112]. Being a sensitive imaging

system, PET enables us to quantitatively understand physiological processes and pathways within the body at a fundamental level. From a therapy standpoint, PET holds probably the greatest potential for the development of theranostic agents. PET images depict the distribution of positron ($\beta^+$ particle)-emitting radionuclides (e.g., fluorine-18 ($^{18}$F), rubidium-82 ($^{82}$Rb), oxygen-15 ($^{15}$O), nitrogen-13 ($^{13}$N), carbon-11 ($^{11}$C), zirconium-89 ($^{89}$Zr), and copper-64 ($^{64}$Cu)) in the body. Emitted positron moves within tissue and deposits its kinetic energy. Upon meeting a free electron in tissue, a mutual annihilation occurs, producing two 511 keV gamma photons (511 keV is the energy equivalent to the rest mass of an electron or positron). These two photons are emitted back-to-back, propagating outward from the site of annihilation 180 degrees apart. Therefore, PET scanners detect a pair of 511 keV photons in what is called annihilation coincidence detection (ACD) in order to obtain projections of radioactivity distribution in the patient. With this approach, only simultaneous gamma rays are detected (with multiple rings of detectors surrounding the patient) and declared as events. A time interval (or time window), typically 2-20 nanoseconds for modern scanners, set by the user determines whether two detected photons are declared as "simultaneous" [113].

The majority of PET systems are coupled to CT scanners (PET/CT systems), though there is a growing interest in PET/MRI systems recently for both clinical pre-clinical studies. By detecting the biodistribution of radiopharmaceuticals in the body, PET studies enable the diagnosis of a wide array of clinical conditions, including cancer, dementia, epilepsy, Parkinsonism as well as cerebrovascular and cardiovascular diseases. There are many PET radiopharmaceuticals, with new radiotracers and their associated ligands being developed extensively [114]. Clinically, the most widely used radiopharmaceutical is $^{18}$F-FDG, which is a glucose analog that detects elevated metabolism in the body [115]. $^{18}$F-FDG PET has also been utilized in the detection of malignant lesions, staging cancer patients as well as assessing tumor treatment response [113]. Typically, the results are reported in the form of a standard uptake value (SUV) which is calculated based on the time of injected dose, the patient or animal's body weight and the radionuclide rate of decay.

Advantages of PET include its high quantitation and sensitivity relative to other modalities and its ability to co-register with CT and MRI. For instance, compared to other radionuclide imaging techniques (e.g., SPECT), PET enables a greater detection sensitivity over a given period of time with its relatively short-lived radionuclides. That is, because PET utilizes radionuclides with shorter physical half-lives compared to SPECT, greater activities can be injected in patients without an increase in the overall radiation. However, PET has several limitations. The most important limitation is poor spatial resolution relative to MRI or CT (**Table 1**). PET also has a relatively high cost with complex equipment, requiring trained personnel and specialized software [116]. Radiation exposure is also a risk to patients [117]. With regard to FDG, one major limitation is that elevated metabolism detected by $^{18}$F-FDG is found in both normal and abnormal tissues which reduces background to noise ratio. This is because there is a typically high baseline glucose utilization in the brain. Pathologic entities that would have high metabolism include abnormal inflammation, tumors, cardiovascular disease, and brain disorders including dementia, epilepsy, Parkinson's disease, stroke, and TBI [118].

As described in the MRI section, $^{18}$F-FDG PET and MRI were combined to study the effects of IN insulin on cerebral glucose uptake, lesion volume, memory and learning, and inflammation using a controlled cortical impact (CCI) TBI model in rats [100]. A significant reduction in $^{18}$F-FDG uptake was observed in the hippocampus on PET imaging along with a significant decrease in the hippocampal lesion volume on MRI, indicating that IN insulin may be a viable therapy for TBI.

Orexin A (hypocretin-1) is one of two isoforms of endogenous neuropeptides produced in the hypothalamus that plays an important role in modulating the sleep/wake cycle, energy and homeostasis, appetite and feeding, drug addiction and cognition [119]. Orexin A can be delivered intranasally with good efficacy [120] and exerts a neuroprotective and anti-inflammatory effect against various CNS disease states [119]. Despite ample evidence that orexin A can be delivered to the CNS intranasally, Van de Bittner et al. was unable to demonstrate CNS delivery following IN administration of

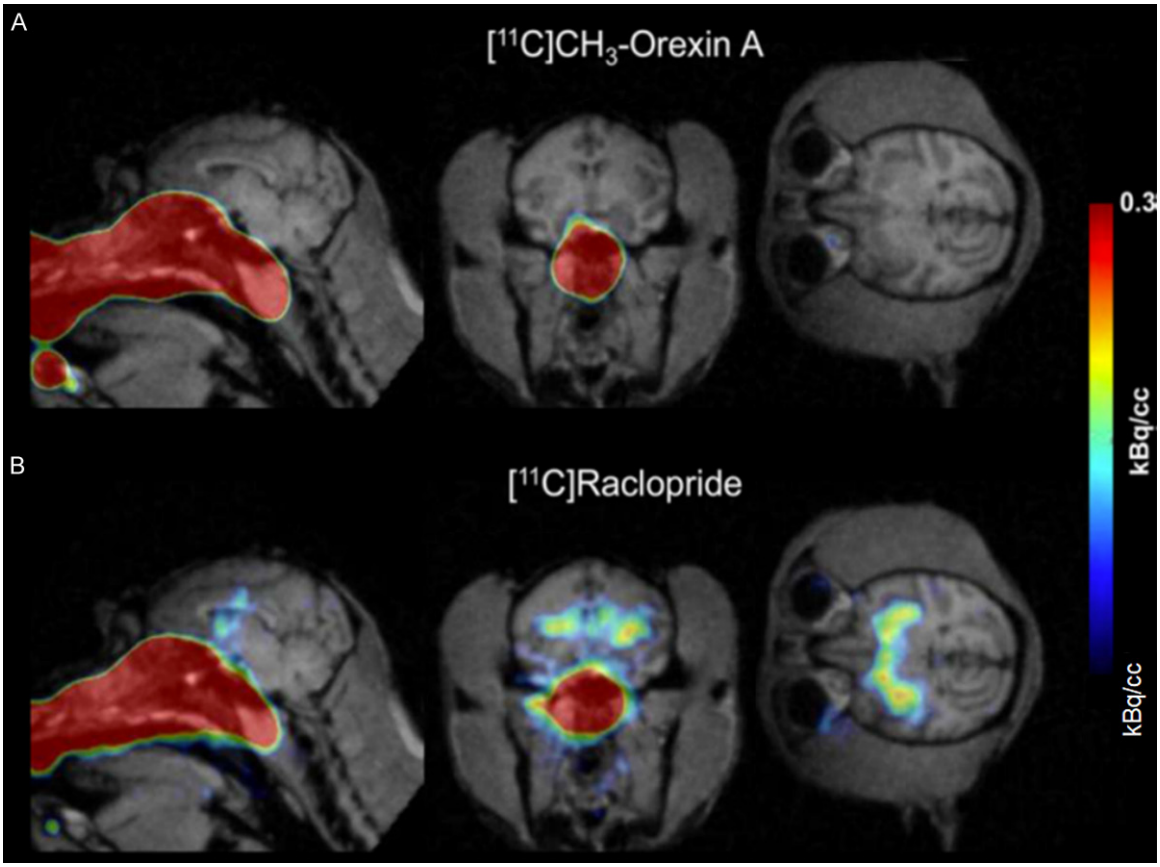


**Figure 5.** PET/MR of $^{11}$C-$CH_3$-Orexin A and $^{11}$C-raclopride in the brain and nasal cavity after intranasal delivery to the neuroepithelium. (Reprinted from ref. 122. Copyright 2018 American Chemical Society) Comparison of $^{11}$C-$CH_3$-Orexin A and $^{11}$C-raclopride uptake in rhesus macaque brain after intranasal administration. $^{11}$C-CH3-Orexin A (A) and $^{11}$C-raclopride (B) were administered using a device for intranasal delivery to the neuroepithelium. At 90 minutes, $^{11}$C-$CH_3$-Orexin A was not visible in the brain using PET/MRI, while $^{11}$C-raclopride was readily visible in the basal ganglia.

a $^{11}$C-radiolabeled form of orexin A ($^{11}$C-$CH_3$-Orexin A) compared with $^{11}$C-raclopride using PET/MR in either rats or non-human primates (**Figure 5**) [121]. Furthermore, in a safety and efficiency trial of a nasal vaccine against botulism, PET imaging of the botulinum type A neurotoxin (BoHc/HA), labeled with $^{18}$F (i.e., $^{18}$F-BoHc/A), did not demonstrate uptake into the cerebrum or olfactory bulb, despite being highly protective against botulism in non-human primates [122]. Nevertheless, PET/CT followed by fusion with MRI was shown in a rat model to be feasible for pharmacokinetic studies using compartmental modeling following IN delivery of the $^{18}$F-FDG radiotracer [123]. The authors were able to generate a time-activity curve after acquiring the data in list-mode from 0.5-30 minutes following IN delivery to demonstrate regional differences in permeability of the radiotracer in the nasal cavity. The authors concluded that absorption and distribution of drug in the rat nasal cavity can be quantitated using PET imaging, but FDG was not detected in the brain after IN delivery. These results are similar to another report that assessed IN delivery of FDG in humans [124]. The reason for this may be saturation of local tissues since these too have glucose transporters that would sequester FDG and prevent more distant perfusion for brain entry.

In a recent clinical trial, an increase in brain metabolic activity was found in patients with Alzheimer's disease and mild cognitive impairment after four months of IN insulin when imaged by PET following IV administration of $^{18}$F-FDG [125]. There was no change in the placebo group. As mentioned earlier, another therapy that is amenable to IN administration is

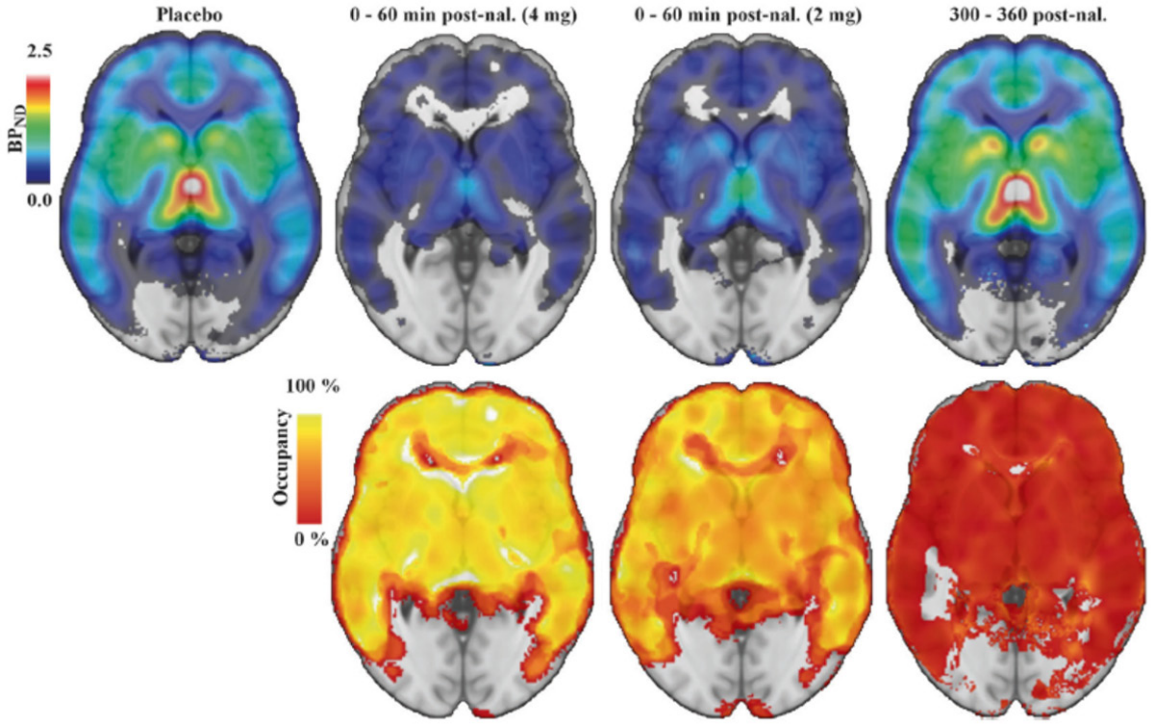


**Figure 6.** $^{11}$C-Carfentanil PET imaging of the brain following intranasal naloxone at 0-60 min or 300-600 min. (Adapted from Johansson et al., 2019). ROI-based binding potential was determined using PET imaging of $^{11}$C-Carfentanil superimposed on a brain MRI template without naloxone administration (upper left image), at 0-60 min following 4 mg of naloxone (upper second image from left), at 0-60 min following 2 mg naloxone (upper third image from left), or at 300-360 min following 2 or 4 mg naloxone. The bottom row indicates percent occupancy of naloxone relative to placebo at the doses administered in the upper row. $BP_{ND}$ is the binding potential of [$^{11}$C] carfentanil relative to the uptake of the tracer in the non-displaceable compartment.

oxytocin. Oxytocin inhibits the amygdala, decreases anxiety and modulates depression and autism when delivered intranasally. Using a radiolabeled partial antagonist to 5-hydroxy-tryptophan-1 receptors and PET/MRI, Mottolese et al. demonstrated in a randomized, double-blind control in humans that oxytocin modulates the serotoninergic system by regulating the 5-hydroxy-tryptophan-1 receptor network, providing an important mechanism of action for oxytocin in humans [126].

Naloxone (Narcan) is a life-saving medication that can rapidly reverse opioid overdose and is available in various forms of administration, including IN [127]. In a study demonstrating the advantages of in vivo imaging, quantitative localization of intranasally delivered naloxone was demonstrated in the brains of 24 healthy male adult human subjects using $^{11}$C-Carfentanil PET imaging combined with brain MRI (**Figure 6**) [128]. Rapid mu opioid receptor occupancy of naloxone following IN delivery was demonstrated directly for the first time in this study and fit well with the rapid (< 5 minutes) reversal of opioid overdose. The authors proposed that naloxone's rapid onset and half-life occupancy of mu opioid receptors of about 100 minutes could be useful for other addictive states such as addictive gambling and alcohol dependence in situations where clinical trials of longer acting mu receptor antagonists have been less efficacious [130].

Zolmitriptan is a selective serotonin 5-HT1B receptor agonist that can be delivered orally or intranasally for the treatment of migraine headaches [129]. When delivered intranasally, the onset of action is detectable within 10 minutes and can quickly abolish major migraine symptoms [130]. Drug biodistribution studies in the nasopharynx, brain, lung, and abdomen were conducted using PET following IN administration of $^{11}$C labelled zolmitriptan ($^{11}$C-zolmitriptan) [131]. In phase 1, the group determined the most appropriate times for PET scanning, whereas in phase 2, they validated the distribution, pharmacokinetics, and tolerability of $^{11}$C-zolmitriptan. Healthy volunteers, aged 18-28 years, were scanned over sectors covering

one of the nasopharynx, brain, lungs or abdomen for up to 1.5 hours post dose by PET. It was determined that most of the $^{11}$C-zolmitriptan was detected in the nasopharynx immediately after IN administration. Moreover, that was a detectable radioactivity within brain tissue, thereby suggesting central penetration of the drug [131].

*Single-photon emission computed tomography*

SPECT is a nuclear tomographic imaging technique that depicts the distribution of gamma-ray-emitting radionuclides (e.g., technetium-99 ($^{99m}$Tc), thallium-201 ($^{201}$Tl), $^{123}$I, and $^{131}$I), acquiring planar (projection) images from multiple angles. These projection images are combined to reconstruct a 3D image depicting the distribution of radionuclides in patients. It depends on radiopharmaceuticals labelled with radionuclides whose radioactive decay produces gamma photons directly. $^{99m}$Tc serves as the workhorse for PET imaging and is the most common radionuclide used due to its short half-life [132]. The most common method of performing SPECT is with a rotating gamma camera mounted on a special gantry that allows up to 360-degree rotation around the patient so that photons are captured in multiple directions. Some recent SPECT systems employ more than one gamma camera head, reducing scan time. In single-head SPECT systems, the gamma camera is rotated either 180 degrees (for most cardiac imaging applications) or 360 degrees (for most non-cardiac imaging applications) so that a standard projection (planar) image is acquired at each angle. Transverse images are reconstructed from the projection data on the system's computer [92]. Like PET, SPECT allows for the freedom to work with other modalities like CT or MRI. Additionally, SPECT scans are far less expensive than PET scans (**Table 1**). However, SPECT is less quantitative than PET. It is also less sensitive than PET because it requires physical collimators that reject photons that are not within a very limited angular range. The collimation requirement in SPECT also introduces noise and increases san time.

At the preclinical level, Esposito et al. tested a $^{99m}$Tc-labeled nanostructured lipid carrier (NLC) (based on a tri-block copolymer platform) distribution using SPECT following IN, intraperitoneal, IV and oral administration in a Wistar rat model as a potential therapeutic application for obesity or other metabolic disorders [133]. The in vivo study demonstrated stability of the NLCs, indicating suitability of the system to carry both drugs and radiotracers for both therapeutic and diagnostic applications. Activity was visualized in the nasal cavity but not in the brain [133]. In addition, Mandlik et al. used $^{99m}$Tc-labelled, zolmitriptan-loaded nanocarriers for in vivo analysis of efficient drug targeting, biodistribution, and kinetics for the treatment of migraines [134]. The anti-migraine zolmitriptan-loaded into radiolabeled nanostructured polymeric carriers and delivered intranasally to Swiss albino mice. The $^{99m}$Tc radiolabelled nanocarriers were efficient in targeting the brain, resulting in higher zolmitriptan-loaded concentrations compared to intranassally delivered unencapsulated free drug solution (i.e., $^{99m}$Tc-zolmitriptan) and intravenously delivered $^{99m}$Tc-labelled, zolmitriptan-loaded nanocarriers. The authors were able to monitor the biodistribution of each therapy by a coupled bimodal SPECT-CT system. Due to the increased radioactivity found in the brain from analysis of the scintigrams and pharmacokinetic parameters, attesting to a more superior drug targeting, it was concluded that intranasally delivered zolmitriptan-loaded nanocarriers are a much more promising system than free drug solution or intravenously delivered drug-loaded nanocarriers.

There are very few available studies specifically utilizing SPECT to study IN delivery in humans. In one study, the clinically approved radiotracer thallium-201 ($^{201}$Tl) was administered intranasally in 24 humans in an attempt to visualize the nose-to-brain route using SPECT/CT fused with MR images of the same subjects [135]. $^{201}$Tl was visualized in the olfactory bulb at 24 hours following IN delivery through the anterior skull base via the cribriform lamina. More recently, olfactory bulb uptake of $^{201}$Tl was demonstrated in healthy human subjects following IN delivery. This was significantly lower in anosmic patients [136] (**Figure 7**). SPECT/MRI with nasal $^{201}$Tl is a dual-modality technique that can be used to assess the olfactory nerve function [136]. In another study, SPECT/MRI was used 24 hours post $^{201}$Tl injection to assess the olfactory nerve connectivity in post-traumatic patients. There was a significant decrease of $^{201}$Tl detection in olfactory-impaired patients [136].

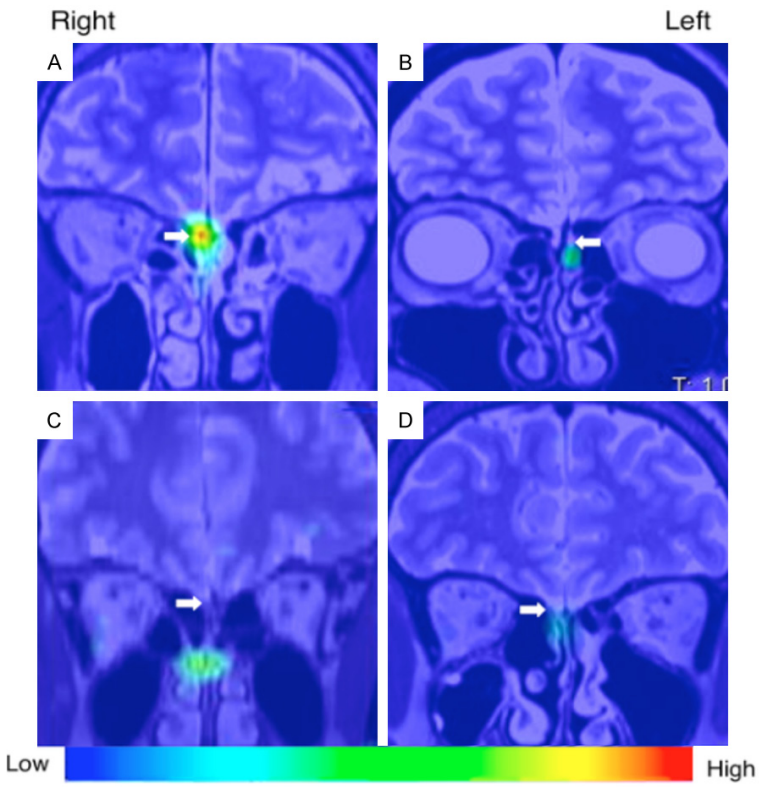


**Figure 7.** SPECT-MR imaging of $^{201}$thallium following intranasal delivery in a human (adapted from Shiga et al., 2013 with permission). Representative SPECT images acquired 24 hours after unilateral intranasal delivery of $^{201}$Tl in 10 healthy volunteers and 21 patients with olfactory dysfunction from various causes. The SPECT images were fused with MRI images from the same patients. $^{201}$Tl was shown to migrate to the olfactory bulb (white arrows) which was significantly correlated with odor recognition thresholds and volume of the olfactory bulb on MRI.

*Gamma scintigraphy*

Gamma scintigraphy is a nuclear medicine imaging approach that uses the same gamma-emitting radiotracers used in SPECT such as $^{99m}$Tc and $^{201}$Tl. The drug-labelled radionuclide (i.e., radiopharmaceutical) emits gamma rays from the organ/tissue where it is localized; these rays are detected by external gamma cameras, forming a 2D projection image which depicts the biodistribution of the gamma-emitting source in the body. Gamma scinitigraphy is often used as an in vivo IN imaging technique preclinically because it is readily available, fast, and inexpensive (**Table 1**). However, some drawbacks include its ability to only produce 2D/planar images, relatively poor spatial resolution compared to MRI or CT, lower detection sensitivity than PET or SPECT, and the deposition of radiation dose.

Recently, ropinerole-loaded mucoadhesive NPs [137], lorazepam-loaded PLGA NPs [138], and risperidone-loaded solid lipid NPs [139], labeled with $^{99m}$Tc, demonstrated greater brain concentrations after IN delivery compared to IV delivery. In a proof-of-concept study, Kakkar et al. reported that circumin-loaded lipid NPs could be visualized in a New Zealand rabbit brain at 4 hours following IN delivery using gamma scintigraphy, but was not visualized in the brain following IV delivery [140]. Unfortunately, the images provided show only a dorsal view without correlational, cross-sectional imaging to distinguish between signals in the nasal cavity versus signal in the brain. Gamma scintigraphy in rats was performed following IN administration of ropinerole hydrochloride-loaded chitosan NPs to ascertain the localization of drug in the brain following IN administration of formulations [137]. The brain-to-blood ratios obtained at 30 minutes are indicative of direct nose-to-brain transport, bypassing the BBB. This study, too, suffered from the lack of verifiable anatomic localization since the nasal cavity cannot be delineated from the brain in these images using planar imaging alone.

One key component to efficient nose-to-brain delivery in humans is the development of a nasal drug delivery device that facilitates focal deposition of the drug onto the dorsal nasal epithelium. Various companies market this ability using various technologies, including bidirectional technology (Optinose™) [141], controlled particle dispersion technology (Kurve Technology) and Precision Olfactory Delivery (POD) technology (Impel Neuropharma) [142]. As an illustration, Optinose developed a breath-powered device with a nasal piece that extends beyond the nasal valve in the nasal cavity. In one study, gamma scintigraphy images were

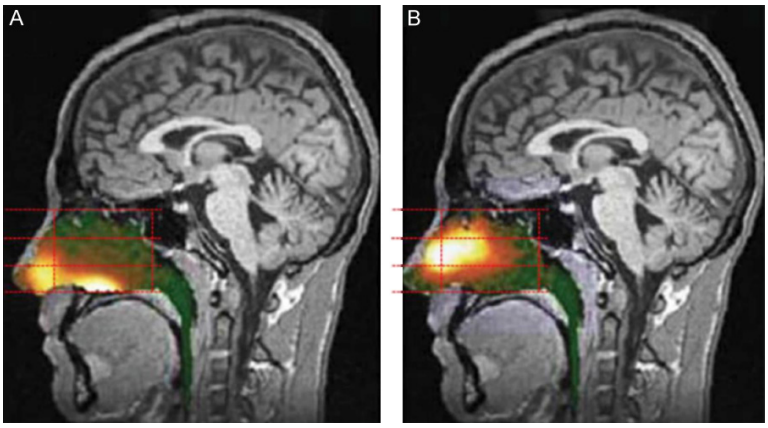


**Figure 8.** Gamma scintigraphy of an example of a breath-powered nasal spray. (Figure included with permission from Djupesland et al., 2013.) Gamma camera images 2 minutes after delivery using a traditional liquid spray (A) and powder with OptiNose Breath-Powered Device (B) shown with a logrithmic hot iron intensity scale. Initial gamma images from one of the subjects are esuperimposed on a lateral MR image. The red dotted lines indicate the segmentation used for regional quantification.

obtained 2 minutes after the delivery of a traditional spray using an Optinose breath-powered device (**Figure 8**) [142]. Images were superimposed on a lateral MRI image. The Optinose breath-powdered device was superior for demonstrating a broader deposition on ciliated respiratory epithelium in the nasal cavity, especially in the upper and middle posterior regions. There was less deposition in non-ciliated nasal regions, which are thought to be less important in nasal drug delivery.

*Computed tomography*

Computed tomography has had a limited role in nose-to-brain drug delivery largely because of its lower soft tissue contrast and lower sensitivity of detection compared to MRI and nuclear medicine, respectively. However, CT has been useful in characterizing the nasal anatomy and dynamic airflow in small animals and humans, which are important for testing IN delivery methods [143]. CT utilizes x-rays to generate cross-sectional, gray-scale images with various pixel (or voxel) intensity values Hounsfield Units (HU) [144]. The degree to which soft tissues attenuate x-ray photons and prohibit them from reaching the detectors determines the image characteristics [145]. CT is widely available, relatively inexpensive, and its images can be acquired quickly compared to other imaging modalities such as MRI (**Table 1**). However, the use of CT involves ionizing radiation, which has the potential for deterministic and stochastic side effects to patients [144, 145], making it not recommended for pregnant women. Also, patients may experience adverse reactions to its iodine- and barium-based contrast agents.

While CT has not been utilized as a standalone imaging modality for IN delivery, it has indeed been used as an adjunct anatomical modality along with dynamic imaging such as PET [123] and SPECT [134]. Furthermore, in animals, the upper and lower airway morphology in Sprague-Dawley rats was studied using micro-CT and image segmentation techniques [146]. The combination of high-resolution, static micro-CT scans with dynamic micro-CT scans was used to assess the deposition patterns of inhaled particles for obligate nose breathers like the rat [146]. In another study, three-dimensional CT was used to study the to pography of the nasal and paranasal sinuses, which were compared with corrosion casting and gross and histologic cross-sections [147]. In humans, Warnken et al. utilized CT to create an anatomical 3D-printed model of the nasal cavity for both pediatric and adult patients to evaluate the deposition pattern of several IN agents [148]. CT was also used for an in vitro model of the nasal cavity to determine the penetration of a nasal spray or the deposition of the olfactory nerve [149, 150]. Furthermore, Shang et al. used CT to reconstruct a human nasal cavity model to better understand mucociliary clearance by examining mucus flow patterns [151]. Often, as mentioned earlier, CT is used in conjunction with other modalities to gain a better understanding of the intra-nasal delivery. In fact, CT can be used for anatomic correlation when combined with PET or SPECT since these modalities have inherently poor anatomic spatial resolution. CT also allows attenuation correction, reducing attenuation artifacts and enabling an improvement in the overall diagnostic performance greater than either modality alone [92].

*Optical imaging*

Optical imaging techniques, particularly BLI and FLI, provide in vivo information at the preclinical level on disease (e.g., tumor) progression [152] and treatment biodistribution [152, 153]. Both BLI and FLI quantify light production for spatial and anatomical information during real-time studies through individual processes [154]. BLI relies on an enzymatic reaction as chemical energy converts into light energy without an excitation source [155]. The complete reaction uses luciferase genes in the presence of a substrate, an energy source and oxygen [154]. Substrates include an endogenous reduced riboflavin phosphate ($FMNH_2$) and long-chain aliphatic aldehyde or exogenous coelenterazine and D-luciferin [152, 154], which can be combined with luciferases such as *Gaussia princeps* luciferase (Gluc) [152, 155] or firefly luciferase (Fluc) [59, 156]. Because of newer cloning and transfection techniques, genes coding for the enzyme and substrate can be introduced into cells for imaging [157]. For example, inserting the *lux* operon into a plasmid or chromosome catalyzes the aldehyde substrate and can be monitored at a wavelength of 490 nm [154]. The absence of required external light makes BLI very favorable since there is a unidirectional full conversion from chemical energy to light [155]. BLI avoids toxic contrast agents, ionizing radiation, high cost, and low throughput associated with other techniques such as MRI or CT [157]. Other advantages include ease of use and little to no background signal except in the abdomen from digested rodent chow-containing chlorophyll [154]. Multiple animals can be imaged at once in a single view, which reduces costs and imaging operation time, and the non-invasiveness of the procedure allows for serial in vivo imaging [157]. A major limitation of BLI, however, is that luciferases often do not permit deep-tissue imaging greater than 1-2 cm [154, 155]. This limitation generally prevents optical imaging from being useful in clinical applications where deeper tissue penetration is a requirement. While optical imaging is one of the most sensitive imaging modalities, improved sensitivity needs to come from imaging advancements as well as modified substrates (**Table 1**). For example, NanoLuc is meant to have improved stability as well as increased luminescence; however, its interaction with mammalian tissues currently challenges its use. One group utilized red-shifted luciferins designed based on the combination of synthetic coelentarazine analogs and NanoLuc mutants to improve such sensitivity [158, 159]. BLI is strongly dependent on substrate administration and, therefore, timing and bioavailability are two important factors [154]. If certain animals require different administration times, cost could become quite expensive. Finally, substrate administration is often via tail vein injection which often requires experienced individuals and could pose a challenge to experiments, especially when working with smaller animals such as mice, if the injection is not done correctly.

In a preclinical model, Fuentes et al. used BLI in order to track the distribution of oncolytic virus-loaded NSCs in the presence of methimazole of fibrin glue as a potential treatment option for glioblastoma [59]. Methimazole and fibrin glue were used to enhance penetration of the olfactory epithelium. NSCs were overexpressed with chemokine receptor type 4 to also facilitate travel to the brain and were modified to be Fluc-expressing for BLI. The cells were administered intranasally and D-luciferin sodium salt was injected intraperitoneally and placed inside each nostril. **Figure 9** represents increased brain localization of NSCs in the presence of methimazole at different time points compared to saline and fibrin glue [59]. In both the saline and the fibrin glue groups, it is clear the NSCs either cleared or remained in the nasal cavity. **Figure 9** has been chosen as a representative BLI image because of its sharp resolution and its change longitudinally. BLI images of the brain are often challenging to acquire in mouse models as it is challenging to discern between the nasal cavity and brain. However, here as time continues, the region of interest shrinks and becomes more concentrated at the brain and this evident shift discerns between the two regions.

FLI is a two-step process as it requires an external light with an appropriate wavelength to excite a fluorescent molecule (fluorophore). This fluorophore is excited to a higher energy state and as the molecule relaxes, light is emitted at a different wavelength than the excitation wavelength [154, 157]. There are a variety of proteins that can be used for FLI including

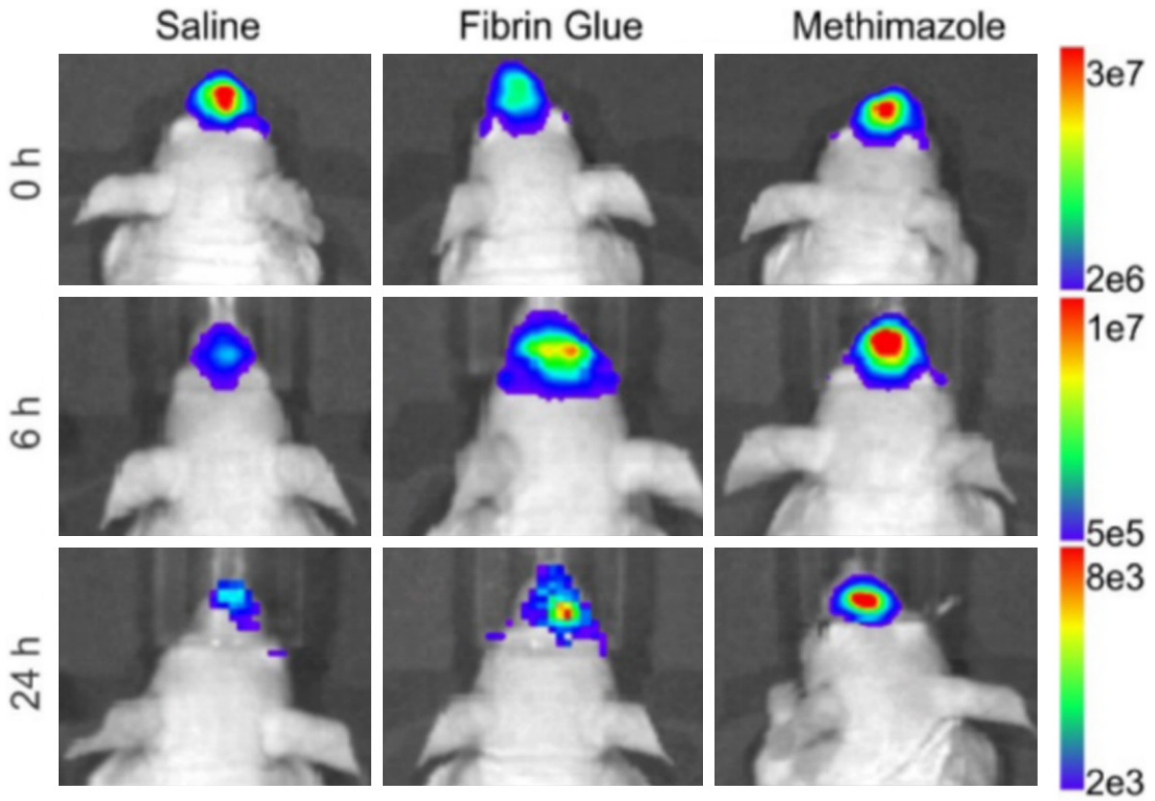


**Figure 9.** In vivo BLI after IN delivery of NSCs. (Figure adapted, with permission, from Spencer et al., 2019) Oncolytic, virus-loaded NSCs were intranasally delivered in the presence of either fibrin glue, methimazole, or saline. Their distribution was monitored over time using BLI. Methimazole best disrupts the olfactory epithelium to facilitate nose-to-brain transition for the treatment of glioblastoma which is seen from the increased concentration and localized region of interest at the brain.

green fluorescent protein (GFP) [152, 160], Turbo red fluorescent protein (TurboRFP) [154], and mCherry fluorescent protein [152], in addition to metals such as gold [161]. Some advantages of FLI include exquisite sensitivity and specificity, high temporal and spatial resolution, availability, easy to operate and inexpensive (**Table 1**) [157]. FLI also does not involve ionizing radiation and is extremely fast in vivo, with measureable signal available within seconds [154]. On the other hand, FLI has disadvantages such as a smaller limit of detection/penetration depth of only a few millimeters compared to that of BLI and background autofluorescence [154].

Fluorescent molecules can be conjugated to a wide variety of entities, including cells and NPs. For example, Bagheri-Mohammed et al. tagged human endometrium-derived stem cells (HEDSCs) with GFP for a possible treatment of Parkinson's disease [160]. The HEDSCs were administered intranasally and ex vivo fluorescence imaging was performed. It was found that the HEDSCs were able to migrate to the substantia nigra pars compacta and behavior was improved [160]. Another group fluorescently labelled poly(*N*-vinyl pyrrolidone)-based nanogels that were attached to insulin for the treatment of Alzheimer's disease [47]. By fluorescently labelling the nanogel, the group was able to monitor biodistribution and clearance and determine that the mucosa was not altered and brain activity was enhanced [47].

FLI and BLI can be used together to provide more information. In a very interesting study, Carvalho et al. used both FLI and BLI to monitor the distribution of olfactory ensheathing cells (OECs) and their role as a carrier for gene therapy in the treatment of glioblastoma [152]. OECs were modified to carry a fusion protein between cytosine deaminase and uracil phosphoribosyl transferase which converts the pro-

drug 5-fluorocytosine into its cytotoxic metabolite. OECs and OECs labelled with the fusion protein were engineered to express Gluc, while glioblastoma stem cells were modified to express Fluc for an in vitro BLI study measuring viability using two separate substrates, coelenterazine and D-luciferin, respectively. An in vivo BLI study combined with an ex vivo FLI study using the same cell modifications showed a decrease in tumor size in the presence of labelled OECs and 5-fluorocytosine as well as migration of both OECs using the nasal pathway into the glioma site [152]. Briefly, mice were injected with glioma stem cells expressing Fluc and mCherry fluorescent protein and one week later were intranasally administered OECs and labelled OECs expressing Gluc and GFP. The mice were then treated daily with an intraperitoneal injection of 5-fluorocytosine. D-luciferin was injected intraperitoneally at 150 μg per gram of body weight and imaged ten minutes later. The fluorescent proteins were utilized in an ex vivo FLI study to confirm migration to the primary tumor site [152].

Another special type of optical imaging, known as photoacoustic (PA) imaging, takes advantage of short light pulses to excite a region of interest (i.e., absorbing medium), causing a slight temperature rise (in the millikelvin range) and thermoelastic expansion [162]. Consequently, pressure waves emitted at ultrasonic frequencies are recorded by a diagnostic ultrasound transducer that produces a 3D image of the absorbing medium distribution. Compared to traditional optical imaging, this imaging approach provides deeper tissue penetration (up to 5-6 cm) and offers higher resolution due to the weaker tissue scattering of ultrasound waves [162]. By virtue of its capability in visualizing the optical absorption properties of biologic tissues, PA imaging also provides higher tissue contrast than conventional ultrasound imaging (**Table 1**) [163]. Additionally, PA imaging utilizes a nonionizing electromagnetic radiation, similar to BLI and FLI.

Near-infrared (NIR, 650-900 nm) absorptive materials are used as contrast agents to improve PA imaging sensitivity and tissue penetration results [164]. Some studies have used PA with NIR NPs for contrast enhancement, tumor targeting, or multimodal imaging [164]. One study, particularly, incorporated a gold nanorod (GNR) into porous magnetic nanoshells [165]. The highly preserved plasmonic feature of GNRs enabled photothermal-induced PA imaging. Doxorubicin, as a model anticancer drug, was loaded into GNR nanocapsules and, under the guidance of MRI/PA dual-modal imaging and magnetic tumor targeting, a photothermal-chemo synergistic therapy was conducted via NIR laser for a highly efficient tumor eradication. It was shown by H&E stained images, blood parameters, and the bodyweight of treated groups that the NPs were well tolerated [165]; however, the nonbiodegradability and potential long-term toxicity of these nanomaterials impact their clinical translation. Data regarding PA-assisted IN drug delivery remain to be explored.

*Conclusions, perspectives and future directions*

IN delivery to the brain can be evaluated with in vivo imaging to determine the fate of agents administered through this route and to assess the progression of diseases as well as the effectiveness of therapeutics. Various in vivo imaging techniques have been discussed in this review, highlighting the critical role imaging plays in the assessment of treatment efficacy. This review also discussed the nose-to-brain route as well as preclinical and clinical IN therapies including small molecules, macromolecular agents, nanosystems, cellular therapies and theranostics.

Innovative IN therapies are continuously being developed. Therefore, we believe that there will be an increasingly growing interest and devoted efforts to not only optimize current imaging methodologies but also develop new diagnostic capabilities in order to facilitate the discovery and clinical translation of novel IN therapies to the brain. In particular, molecular and multimodality imaging techniques will likely continue to be at the forefront of development, dominating the aforementioned efforts. PET/MRI, for instance, is an emerging molecular imaging modality that harnesses the strengths of both PET and MRI to produce hybrid quantitative images with exquisite soft tissue contrast. Therefore, we believe, PET/MRI in IN delivery studies is and will continue to be a promising area of research and investigation with a potentially significant clinical impact in the future.

In addition to optimizing and developing imaging capabilities to facilitate IN delivery, future work should investigate strategies that enhance the delivery of drugs across the nasal barriers providing a more localized delivery to specific brain sites. One of these strategies is focused ultrasound (FUS), which is a noninvasive, therapeutic modality that harnesses the mechanical and thermal effects of ultrasonic beams focused at a region of interest in order to induce therapeutic benefits in deep-seated tissues with little or no harm to intervening tissues. FUS, which is FDA approved for certain clinical conditions, has already demonstrated promising initial results supporting its capability in enhancing the efficacy of IN delivery within targeted brain regions [166, 167]. The FUS-mediated transport enhancement of intranasally administered agents utilizes another FDA-approved component, namely microbubbles, in order to induce mechanical effects (cavitation) that facilitate the transport of therapeutics in the brain.

We also believe that combination therapy, delivered intranasally using a NP-based drug delivery system, can bring about significant advantages in treating debilitating brain diseases over single-drug therapies. Moreover, engineering multifunctional NP-based delivery systems that not only incorporate multiple anticancer drugs but also imaging agents as well as targeting moieties would certainly provide added advantages in IN delivery. Such a nanotheranostic platform can enable targeted, image-guided IN delivery to the brain, utilizing one or more of the diagnostic imaging modalities discussed in this review for treatment planning, real-time monitoring and control, as well as posttreatment evaluation of efficacy.

## Acknowledgements

The authors would also like to thank Dr. Jason Parker for fruitful discussions. We would also like to thank the Joseph Acchiardo and Philip Marcadis who contributed to reference and data gathering.

## Disclosure of conflict of interest

None.

## Abbreviations

11C, Carbon-11; 13N, Nitrogen-13; 15O, Oxygen-15; 18F, Fluorine-18; 18F-FDG, Fluorine-18 Fluorodeoxyglucose; 64Cu, Copper-64; 68Ga, Gallium-68; 82Rb, Rubidium-82; 89Zr, Zirconium-89; 90Y, Yttrium-90; 99mTc, Technetium-99; 123I, Iodine-123; 131I, Iodine-131; 177Lu, Lutetium-177; 201Tl, Thallium-201; ACD, Annihilation coincidence detection; ADHD, Attention-deficit/hyperactivity disorder; ADNP, Activity-dependent neuroprotective protein; BBB, Blood-brain barrier; BLI, Bioluminescence imaging; BMSC, Bone marrow-derived stem cell; BoHc/A, 18F-Clostridium botulinum type A neurotoxin; CCI, Controlled cortical impact; CNS, Central nervous system; CSF, Cerebral spinal fluid; CT, Computed tomography; DTI, Diffusion tensor imaging; DWI, Diffusion-weighted imaging; FLASH, Fast low-angle shot; FLI, Fluorescence imaging; Fluc, Firefly luciferase; FUS, Focused ultrasound; Gd-DTPA, Gadolinium-diethylenetriamine pentaacetic acid; GFP, Green fluorescent protein; Gluc, Gaussia princeps luciferase; GNR, Gold nanorod; GRE, Gradient recalled echo; GRAS, Generally regarded as safe; HEDSCs, Human endometrium-derived stem cells; HU, Hounsfield units; IN, Intranasal; IV, Intravenous; IL-4, Interleukin-4; MCA, Middle Cerebral Artery; MIBG, Metaiodobenzylguanidine; MOG, Myelin oligodendrocyte glycoprotein; MPIO, Micron-sized iron oxide particles; MPRAGE, Magnetization Prepared Rapid Gradient Echo; MRI, Magnetic resonance imaging; fMRI, Functional MRI; MSC, Mesenchymal stem cell; MTD, Maximum tolerated dose; NE, Nanoemulsion; NIR, Near-infrared; NLC, Nanostructured lipid carrier; NPs, Nanoparticles; NSC, Neural stem cell; NSPC, Neural stem/progenitor cell; OEC, Olfactory ensheathing cell; PA, Photoacoustic; PEG, Polyethylene glycol; PLGA, Poly(lactic-co-glycolic acid); PET, Positron emission tomography; POD, Precision olfactory delivery; PSMA, Prostate specific membrane antigen (PSMA); PTSD, Post-traumatic stress disorder; RARE, Rapid acquisition with relaxation enhancement; RF, Radiofrequency; SPECT, Single-photon emission computed tomography; SUV, Standard uptake value; SNR, Signal-to-noise ratio; SPION, Superparamagnetic iron oxide nanoparticles; SWI, Susceptibility-weighted imaging; TBI, Traumatic brain injury; Technetium-99, 99m-Tc; Thallium-201, 201Tl; TNF, Tumor necrosis factor; TRAIL, TNF-related apoptosis-inducing ligand; Turbo RFP, Turbo red fluorescent protein.

**Address correspondence to:** Dr. Michael C Veronesi, Department of Radiology and Imaging Sciences,

Indiana University School of Medicine, Research 2 Building (R2), Room E174, 950 W. Walnut Street, Indianapolis, IN 46202-5181, USA. Tel: 317-278-9848; E-mail: mverones@iu.edu

## References


[1] Abbott NJ. Blood-brain barrier structure and function and the challenges for CNS drug delivery. J Inherit Metab Dis 2013; 36: 437-449.

[2] Pardridge WM. CSF, blood-brain barrier, and brain drug delivery. Expert Opin Drug Deliv 2016; 13: 963-975.

[3] Ganger S and Schindowski K. Tailoring formulations for intranasal nose-to-brain delivery: a review on architecture, physico-chemical characteristics and mucociliary clearance of the nasal olfactory mucosa. Pharmaceutics 2018; 10.

[4] Lochhead JJ and Thorne RG. Intranasal delivery of biologics to the central nervous system. Adv Drug Deliv Rev 2012; 64: 614-628.

[5] lochhead J and Thorne RG. Intranasal drug delivery to the brain. Drug delivery to the brain. New York: Springer; 2014. pp.401-431.

[6] Pardridge WM. Drug targeting to the brain. Pharm Res 2007; 24: 1733-1744.

[7] Gilmore JL, Yi X, Quan L and Kabanov AV. Novel nanomaterials for clinical neuroscience. J Neuroimmune Pharmacol 2008; 3: 83-94.

[8] Tosi G, Ruozi B and Belletti D. Nanomedicine: the future for advancing medicine and neuroscience. Nanomedicine (Lond) 2012; 7: 1113-1116.

[9] Clerico DM, To WC and Lanza DC. Anatomy of the human nasal passages. In: Doty RL, editor. Handbook of olfaction and gustation. 3rd edition. Hoboken, New Jersey: Wiley Blackwell; 2015. pp. xviii, 1217.

[10] Harkema JR. Comparative aspects of nasal airway anatomy: relevance to inhalation toxicology. Toxicol Pathol 1991; 19: 321-336.

[11] Ding X DA. Composition, enzymatic location and metabolish. In: Doty RL, editor. Handbook of olfaction and gustation. 3rd edition. Hoboken, New Jersey: Wiley Blackwell; 2015. pp. xviii, 1217.

[12] Ghadiri M, Young PM and Traini D. Strategies to enhance drug absorption via nasal and pulmonary routes. Pharmaceutics 2019; 11.

[13] Ross TM, Martinez PM, Renner JC, Thorne RG, Hanson LR and Frey WH 2nd. Intranasal administration of interferon beta bypasses the blood-brain barrier to target the central nervous system and cervical lymph nodes: a non-invasive treatment strategy for multiple sclerosis. J Neuroimmunol 2004; 151: 66-77.

[14] Thorne RG, Pronk GJ, Padmanabhan V and Frey WH 2nd. Delivery of insulin-like growth factor-I to the rat brain and spinal cord along olfactory and trigeminal pathways following intranasal administration. Neuroscience 2004; 127: 481-496.

[15] Lochhead JJ, Wolak DJ, Pizzo ME and Thorne RG. Rapid transport within cerebral perivascular spaces underlies widespread tracer distribution in the brain after intranasal administration. J Cereb Blood Flow Metab 2015; 35: 371-381.

[16] Thorne RG, Hanson LR, Ross TM, Tung D and Frey WH 2nd. Delivery of interferon-beta to the monkey nervous system following intranasal administration. Neuroscience 2008; 152: 785-797.

[17] Lochhead JJ, Kellohen KL, Ronaldson PT and Davis TP. Distribution of insulin in trigeminal nerve and brain after intranasal administration. Sci Rep 2019; 9: 2621.

[18] Illum L. Is nose-to-brain transport of drugs in man a reality? J Pharm Pharmacol 2004; 56: 3-17.

[19] Djupesland PG, Messina JC and Mahmoud RA. The nasal approach to delivering treatment for brain diseases: an anatomic, physiologic, and delivery technology overview. Ther Deliv 2014; 5: 709-733.

[20] Leopold DA, Hummel T, Schwob JE, Hong SC, Knecht M and Kobal G. Anterior distribution of human olfactory epithelium. Laryngoscope 2000; 110: 417-421.

[21] Balin BJ, Broadwell RD, Salcman M and el-Kalliny M. Avenues for entry of peripherally administered protein to the central nervous system in mouse, rat, and squirrel monkey. J Comp Neurol 1986; 251: 260-280.

[22] Fortuna A, Alves G, Serralheiro A, Sousa J and Falcao A. Intranasal delivery of systemic-acting drugs: small-molecules and biomacromolecules. Eur J Pharm Biopharm 2014; 88: 8-27.

[23] Erdő F, Bors LA, Farkas D, Bajza Á and Gizurarson S. Evaluation of intranasal delivery route of drug administration for brain targeting. Brain Research Bulletin 2018; 143: 155-170.

[24] Corrigan M, Wilson SS and Hampton J. Safety and efficacy of intranasally administered medications in the emergency department and prehospital settings. Am J Health Syst Pharm 2015; 72: 1544-1554.

[25] Chen W, Silverman DH, Delaloye S, Czernin J, Kamdar N, Pope W, Satyamurthy N, Schiepers C and Cloughesy T. 18F-FDOPA PET imaging of brain tumors: comparison study with 18F-FDG PET and evaluation of diagnostic accuracy. J Nucl Med 2006; 47: 904-911.

[26] Claxton A, Baker LD, Hanson A, Trittschuh EH, Cholerton B, Morgan A, Callaghan M, Arbuckle M, Behl C and Craft S. Long acting intranasal

insulin detemir improves cognition for adults with mild cognitive impairment or early-stage Alzheimer's disease dementia. J Alzheimers Dis 2015; 45: 1269-1270.
[27] Ostrom QT, Gittleman H, Xu J, Kromer C, Wolinsky Y, Kruchko C and Barnholtz-Sloan JS. CBTRUS statistical report: primary brain and other central nervous system tumors diagnosed in the united states in 2009-2013. Neuro Oncol 2016; 18: v1-v75.
[28] Kalia LV, Kalia SK and Lang AE. Disease-modifying strategies for Parkinson's disease. Mov Disord 2015; 30: 1442-1450.
[29] Lee SY, Lee AR, Hwangbo R, Han J, Hong M and Bahn GH. Is oxytocin application for autism spectrum disorder evidence-based? Exp Neurobiol 2015; 24: 312-324.
[30] Chien LN, Ostrom QT, Gittleman H, Lin JW, Sloan AE, Barnett GH, Elder JB, McPherson C, Warnick R, Chiang YH, Lin CM, Rogers LR, Chiou HY and Barnholtz-Sloan JS. International differences in treatment and clinical outcomes for high grade glioma. PLoS One 2015; 10: e0129602.
[31] Kromer C, Xu J, Ostrom QT, Gittleman H, Kruchko C, Sawaya R and Barnholtz-Sloan JS. Estimating the annual frequency of synchronous brain metastasis in the United States 2010-2013: a population-based study. J Neurooncol 2017; 134: 55-64.
[32] Ostrom QT, Gittleman H, Kruchko C and Barnholtz-Sloan JS. Primary brain and other central nervous system tumors in Appalachia: regional differences in incidence, mortality, and survival. J Neurooncol 2018; 142: 27-38.
[33] Ostrom QT, Gittleman H, Kruchko C, Louis DN, Brat DJ, Gilbert MR, Petkov VI and Barnholtz-Sloan JS. Completeness of required site-specific factors for brain and CNS tumors in the surveillance, epidemiology and end results (SEER) 18 database (2004-2012, varying). J Neurooncol 2016; 130: 31-42.
[34] Sabban EL, Alaluf LG and Serova LI. Potential of neuropeptide Y for preventing or treating post-traumatic stress disorder. Neuropeptides 2016; 56: 19-24.
[35] Chapman CD, Frey WH 2nd, Craft S, Danielyan L, Hallschmid M, Schioth HB and Benedict C. Intranasal treatment of central nervous system dysfunction in humans. Pharm Res 2013; 30: 2475-2484.
[36] Kim HJ, Shin WJ, Park S, Ahn HS and Oh JH. The sedative effects of the intranasal administration of dexmedetomidine in children undergoing surgeries compared to other sedation methods: a systematic review and meta-analysis. J Clin Anesth 2017; 38: 33-39.
[37] Lipton RB, McGinley JS, Shulman KJ, Wirth RJ and Buse DC. Faster improvement in migraine pain intensity and migraine-related disability at early time points with AVP-825 (sumatriptan nasal powder delivery system) versus oral sumatriptan: a comparative randomized clinical trial across multiple attacks from the COMPASS study. Headache 2017; 57: 1570-1582.
[38] Traynor K. Esketamine nasal spray approved for treatment-resistant depression. Am J Health Syst Pharm 2019; 76: 573.
[39] Benfield J and Musto A. Intranasal therapy to stop status epilepticus in prehospital settings. Drugs R D 2018; 18: 7-17.
[40] Sin B, Jeffrey I, Halpern Z, Adebayo A, Wing T, Lee AS, Ruiz J, Persaud K, Davenport L, de Souza S and Williams M. Intranasal sufentanil versus intravenous morphine for acute pain in the emergency department: a randomized pilot trial. J Emerg Med 2019; 56: 301-307.
[41] Rogriguez D, Urrutia G, Escobar Y, Moya J and Murillo M. Efficacy and safety of oral or nasal fentanyl for treatment of breakthrough pain in cancer patients: a systematic review. J Pain Palliat Care Pharmacother 2015; 29: 228-246.
[42] Ryan SA and Dunne RB. Pharmacokinetic properties of intranasal and injectable formulations of naloxone for community use: a systematic review. Pain Manag 2018; 8: 231-245.
[43] Webster LR, Pantaleon C, Shah MS, DiFalco R, Iverson M, Smith MD, Kinzler ER and Aigner S. A randomized, double-blind, double-dummy, placebo-controlled, intranasal drug liking study on a novel abuse-deterrent formulation of morphine-morphine ARER. Pain Med 2017; 18: 1303-1313.
[44] Webster LR, Iverson M, Pantaleon C, Smith MD, Kinzler ER and Aigner S. A randomized, double-blind, double-dummy, placebo-controlled, intranasal human abuse potential study of oxycodone ARIR, a novel, immediate-release, abuse-deterrent formulation. Pain Med 2019; 20: 747-757.
[45] Allison M and Hale C. A phase I study of the pharmacokinetics and pharmacodynamics of intranasal doxylamine in subjects with chronic intermittent sleep impairment. Drugs R D 2018; 18: 129-136.
[46] Pires A, Fortuna A, Alves G and Falcao A. Intranasal drug delivery: how, why and what for? J Pharm Pharm Sci 2009; 12: 288-311.
[47] Picone P, Sabatino MA, Ditta LA, Amato A, San Biagio PL, Mulè F, Giacomazza D, Dispenza C and Di Carlo M. Nose-to-brain delivery of insulin enhanced by a nanogel carrier. J Control Release 2018; 270: 23-36.
[48] Kumar A, Pandey AN and Jain SK. Nasal-nanotechnology: revolution for efficient therapeutics delivery. Drug Deliv 2016; 23: 681-693.

[49] King DF, McKay PF, Mann JF, Jones CB and Shattock RJ. Plasmid DNA vaccine co-immunisation modulates cellular and humoral immune responses induced by intranasal inoculation in mice. PLoS One 2015; 10: e0141557.
[50] Nyombayire J, Anzala O, Gazzard B, Karita E, Bergin P, Hayes P, Kopycinski J, Omosa-Manyonyi G, Jackson A, Bizimana J, Farah B, Sayeed E, Parks CL, Inoue M, Hironaka T, Hara H, Shu T, Matano T, Dally L, Barin B, Park H, Gilmour J, Lombardo A, Excler JL, Fast P, Laufer DS and Cox JH. First-in-human evaluation of the safety and immunogenicity of an intranasally administered replication-competent sendai virus-vectored HIV Type 1 Gag vaccine: induction of potent T-Cell or antibody responses in prime-boost regimens. J Infect Dis 2017; 215: 95-104.
[51] Kendrick KM, Guastella AJ and Becker B. Overview of human oxytocin research. Curr Top Behav Neurosci 2018; 35: 321-348.
[52] Jones C, Barrera I, Brothers S, Ring R and Wahlestedt C. Oxytocin and social functioning. Dialogues Clin Neurosci 2017; 19: 193-201.
[53] Moeini M, Omidi A, Sehat M and Banafshe HR. The effects of oxytocin on withdrawal, craving and stress response in heroin-dependent patients: a randomized, double-blind clinical trial. Eur Addict Res 2019; 25: 41-47.
[54] Fang A, Lawson EA and Wilhelm S. Intranasal oxytocin modulates higher order social cognition in body dysmorphic disorder. Depress Anxiety 2019; 36: 153-161.
[55] Russell J, Maguire S, Hunt GE, Kesby A, Suraev A, Stuart J, Booth J and McGregor IS. Intranasal oxytocin in the treatment of anorexia nervosa: randomized controlled trial during re-feeding. Psychoneuroendocrinology 2018; 87: 83-92.
[56] Kamei N, Shingaki T, Kanayama Y, Tanaka M, Zochi R, Hasegawa K, Watanabe Y and Takeda-Morishita M. Visualization and quantitative assessment of the brain distribution of insulin through nose-to-brain delivery based on the cell-penetrating peptide noncovalent strategy. Mol Pharm 2016; 13: 1004-1011.
[57] Kamei N, Okada N, Ikeda T, Choi H, Fujiwara Y, Okumura H and Takeda-Morishita M. Effective nose-to-brain delivery of exendin-4 via coadministration with cell-penetrating peptides for improving progressive cognitive dysfunction. Sci Rep 2018; 8: 17641.
[58] Appu AP, Arun P, Krishnan JKS, Moffett JR and Namboodiri AMA. Rapid intranasal delivery of chloramphenicol acetyltransferase in the active form to different brain regions as a model for enzyme therapy in the CNS. J Neurosci Methods 2016; 259: 129-134.
[59] Spencer D, Yu D, Morshed RA, Li G, Pituch KC, Gao DX, Bertolino N, Procissi D, Lesniak MS and Balyasnikova IV. Pharmacologic modulation of nasal epithelium augments neural stem cell targeting of glioblastoma. Theranostics 2019; 9: 2071-2083.
[60] Bonferoni MC, Rossi S, Sandri G, Ferrari F, Gavini E, Rassu G and Giunchedi P. Nanoemulsions for "nose-to-brain" drug delivery. Pharmaceutics 2019; 11: 84.
[61] Chavda VP. Chapter 4 - Nanobased nano drug delivery: a comprehensive review. In: Mohapatra SS, Ranjan S, Dasgupta N, Mishra RK, Thomas S, editors. Applications of Targeted Nano Drugs and Delivery Systems. Elsevier; 2019. pp. 69-92.
[62] Patra JK, Das G, Fraceto LF, Campos EVR, Rodriguez-Torres MDP, Acosta-Torres LS, Diaz-Torres LA, Grillo R, Swamy MK, Sharma S, Habtemariam S and Shin HS. Nano based drug delivery systems: recent developments and future prospects. J Nanobiotechnology 2018; 16: 71.
[63] de Oliveira Junior ER, Nascimento TL, Salomao MA, da Silva ACG, Valadares MC and Lima EM. Increased nose-to-brain delivery of melatonin mediated by polycaprolactone nanoparticles for the treatment of glioblastoma. Pharm Res 2019; 36: 131.
[64] Bobo D, Robinson KJ, Islam J, Thurecht KJ and Corrie SR. Nanoparticle-based medicines: a review of FDA-approved materials and clinical trials to date. Pharm Res 2016; 33: 2373-2387.
[65] Mohanraj VJ and Chen Y. Nanoparticles - a review. Trop J Pharm Res 2007; 5: 561-573.
[66] Mi P, Cabral H, Kokuryo D, Rafi M, Terada Y, Aoki I, Saga T, Takehiko I, Nishiyama N and Kataoka K. Gd-DTPA-loaded polymer-metal complex micelles with high relaxivity for MR cancer imaging. Biomaterials 2013; 34: 492-500.
[67] Zhang L, Chan JM, Gu FX, Rhee JW, Wang AZ, Radovic-Moreno AF, Alexis F, Langer R and Farokhzad OC. Self-assembled lipid--polymer hybrid nanoparticles: a robust drug delivery platform. ACS Nano 2008; 2: 1696-1702.
[68] Belhadj Z, Zhan C, Ying M, Wei X, Xie C, Yan Z and Lu W. Multifunctional targeted liposomal drug delivery for efficient glioblastoma treatment. Oncotarget 2017; 8: 66889-66900.
[69] Eatemadi A, Daraee H, Zarghami N, Yar HM and Akbarzadeh A. Nanofiber: synthesis and biomedical applications. Artif Cells Nanomed Biotechnol 2016; 44: 111-121.
[70] Borran AA, Aghanejad A, Farajollahi A, Barar J and Omidi Y. Gold nanoparticles for radiosensitizing and imaging of cancer cells. Radiation Physics and Chemistry 2018; 152: 137-144.
[71] Chatterjee B, Gorain B, Mohananaidu K, Sengupta P, Mandal UK and Choudhury H.

Targeted drug delivery to the brain via intranasal nanoemulsion: available proof of concept and existing challenges. Int J Pharm 2019; 565: 258-268.
[72] Colombo M, Figueiró F, de Fraga Dias A, Teixeira HF, Battastini AMO and Koester LS. Kaempferol-loaded mucoadhesive nanoemulsion for intranasal administration reduces glioma growth in vitro. Int J Pharm 2018; 543: 214-223.
[73] Galeano C, Qiu Z, Mishra A, Farnsworth SL, Hemmi JJ, Moreira A, Edenhoffer P and Hornsby PJ. The route by which intranasally delivered stem cells enter the central nervous system. Cell Transplant 2018; 27: 501-514.
[74] Li G, Bonamici N, Dey M, Lesniak MS and Balyasnikova IV. Intranasal delivery of stem cell-based therapies for the treatment of brain malignancies. Expert Opin Drug Deliv 2018; 15: 163-172.
[75] Danielyan L, Schafer R, von Ameln-Mayerhofer A, Bernhard F, Verleysdonk S, Buadze M, Lourhmati A, Klopfer T, Schaumann F, Schmid B, Koehle C, Proksch B, Weissert R, Reichardt HM, van den Brandt J, Buniatian GH, Schwab M, Gleiter CH and Frey WH 2nd. Therapeutic efficacy of intranasally delivered mesenchymal stem cells in a rat model of Parkinson disease. Rejuvenation Res 2011; 14: 3-16.
[76] Danielyan L, Beer-Hammer S, Stolzing A, Schafer R, Siegel G, Fabian C, Kahle P, Biedermann T, Lourhmati A, Buadze M, Novakovic A, Proksch B, Gleiter CH, Frey WH and Schwab M. Intranasal delivery of bone marrow-derived mesenchymal stem cells, macrophages, and microglia to the brain in mouse models of Alzheimer's and Parkinson's disease. Cell Transplant 2014; 23 Suppl 1: S123-139.
[77] Yu-Taeger L, Stricker-Shaver J, Arnold K, Bambynek-Dziuk P, Novati A, Singer E, Lourhmati A, Fabian C, Magg J, Riess O, Schwab M, Stolzing A, Danielyan L and Nguyen HHP. Intranasal administration of mesenchymal stem cells ameliorates the abnormal dopamine transmission system and inflammatory reaction in the R6/2 mouse model of huntington disease. Cells 2019; 8.
[78] Wei N, Yu SP, Gu X, Taylor TM, Song D, Liu XF and Wei L. Delayed intranasal delivery of hypoxic-preconditioned bone marrow mesenchymal stem cells enhanced cell homing and therapeutic benefits after ischemic stroke in mice. Cell Transplant 2013; 22: 977-991.
[79] Chau MJ, Deveau TC, Gu X, Kim YS, Xu Y, Yu SP and Wei L. Delayed and repeated intranasal delivery of bone marrow stromal cells increases regeneration and functional recovery after ischemic stroke in mice. BMC Neurosci 2018; 19: 20.
[80] van Velthoven CT, Kavelaars A, van Bel F and Heijnen CJ. Nasal administration of stem cells: a promising novel route to treat neonatal ischemic brain damage. Pediatr Res 2010; 68: 419-422.
[81] Wei ZZ, Gu X, Ferdinand A, Lee JH, Ji X, Ji XM, Yu SP and Wei L. Intranasal delivery of bone marrow mesenchymal stem cells improved neurovascular regeneration and rescued neuropsychiatric deficits after neonatal stroke in rats. Cell Transplant 2015; 24: 391-402.
[82] Reitz M, Demestre M, Sedlacik J, Meissner H, Fiehler J, Kim SU, Westphal M and Schmidt NO. Intranasal delivery of neural stem/progenitor cells: a noninvasive passage to target intracerebral glioma. Stem Cells Transl Med 2012; 1: 866-873.
[83] Balyasnikova IV, Prasol MS, Ferguson SD, Han Y, Ahmed AU, Gutova M, Tobias AL, Mustafi D, Rincon E, Zhang L, Aboody KS and Lesniak MS. Intranasal delivery of mesenchymal stem cells significantly extends survival of irradiated mice with experimental brain tumors. Mol Ther 2014; 22: 140-148.
[84] Soria B, Martin-Montalvo A, Aguilera Y, Mellado-Damas N, Lopez-Beas J, Herrera-Herrera I, Lopez E, Barcia JA, Alvarez-Dolado M, Hmadcha A and Capilla-Gonzalez V. Human mesenchymal stem cells prevent neurological complications of radiotherapy. Front Cell Neurosci 2019; 13: 204.
[85] Dey M, Yu D, Kanojia D, Li G, Sukhanova M, Spencer DA, Pituch KC, Zhang L, Han Y, Ahmed AU, Aboody KS, Lesniak MS and Balyasnikova IV. Intranasal oncolytic virotherapy with CXCR4-Enhanced stem cells extends survival in mouse model of glioma. Stem Cell Reports 2016; 7: 471-482.
[86] Ding H, Wu F and Nair MP. Image-guided drug delivery to the brain using nanotechnology. Drug Discov Today 2013; 18: 1074-1080.
[87] Yordanova A, Eppard E, Kurpig S, Bundschuh RA, Schonberger S, Gonzalez-Carmona M, Feldmann G, Ahmadzadehfar H and Essler M. Theranostics in nuclear medicine practice. Onco Targets Ther 2017; 10: 4821-4828.
[88] Lee DY and Li KC. Molecular theranostics: a primer for the imaging professional. AJR Am J Roentgenol 2011; 197: 318-324.
[89] Nguyen QT, Lee EJ, Huang MG, Park YI, Khullar A and Plodkowski RA. Diagnosis and treatment of patients with thyroid cancer. Am Health Drug Benefits 2015; 8: 30-40.
[90] Sukumar UK, Bose RJC, Malhotra M, Babikir HA, Afjei R, Robinson E, Zeng Y, Chang E, Habte F, Sinclair R, Gambhir SS, Massoud TF and Paulmurugan R. Intranasal delivery of targeted

polyfunctional gold-iron oxide nanoparticles loaded with therapeutic microRNAs for combined theranostic multimodality imaging and presensitization of glioblastoma to temozolomide. Biomaterials 2019; 218: 119342.
[91] Radue EW, Weigel M, Wiest R and Urbach H. Introduction to magnetic resonance imaging for neurologists. Continuum (Minneap Minn) 2016; 22: 1379-1398.
[92] Bushberg JT, Seibert JA, Leidholdt EM and Boone JM. The essential physics of medical imaging. Wolters Kluwer Health 2011.
[93] Hendrick RE and Haacke MM. Basic physics of MR contrast agents and maxmization of image contrast. J Magn Reson Imaging 1993; 3: 137-148.
[94] Okuhata Y. Delivery of diagnostic agents for magnetic resonance imaging. Adv Drug Deliv Rev 1999; 37: 121-137.
[95] Zhang Q, Zhu W, Xu F, Dai X, Shi L, Cai W, Mu H, Hitchens TK, Foley LM, Liu X, Yu F, Chen J, Shi Y, Leak RK, Gao Y, Chen J and Hu X. The interleukin-4/PPARgamma signaling axis promotes oligodendrocyte differentiation and remyelination after brain injury. PLoS Biol 2019; 17: e3000330.
[96] Sragovich S, Malishkevich A, Piontkewitz Y, Giladi E, Touloumi O, Lagoudaki R, Grigoriadis N and Gozes I. The autism/neuroprotection-linked ADNP/NAP regulate the excitatory glutamatergic synapse. Transl Psychiatry 2019; 9: 2.
[97] Levy Barazany H, Barazany D, Puckett L, Blanga-Kanfi S, Borenstein-Auerbach N, Yang K, Peron JP, Weiner HL and Frenkel D. Brain MRI of nasal MOG therapeutic effect in relapsing-progressive EAE. Exp Neurol 2014; 255: 63-70.
[98] Yadav S, Pawar G, Kulkarni P, Ferris C and Amiji M. CNS delivery and anti-inflammatory effects of intranasally administered cyclosporine-A in cationic nanoformulations. J Pharmacol Exp Ther 2019; 370: 843-854.
[99] Chen Y, Fan H, Xu C, Hu W and Yu B. Efficient cholera toxin B Subunit-Based nanoparticles with MRI capability for drug delivery to the brain following intranasal administration. Macromol Biosci 2019; 19: e1900017.
[100] Brabazon F, Wilson CM, Jaiswal S, Reed J, Frey WH Nd and Byrnes KR. Intranasal insulin treat ment of an experimental model of moderate traumatic brain injury. J Cereb Blood Flow Metab 2017; 37: 3203-3218.
[101] Das M, Wang C, Bedi R, Mohapatra SS and Mohapatra S. Magnetic micelles for DNA delivery to rat brains after mild traumatic brain injury. Nanomedicine 2014; 10: 1539-1548.
[102] Santiago JCP and Hallschmid M. Outcomes and clinical implications of intranasal insulin administration to the central nervous system. Exp Neurol 2019; 317: 180-190.
[103] Ding C, Leow MK and Magkos F. Oxytocin in metabolic homeostasis: implications for obesity and diabetes management. Obes Rev 2019; 20: 22-40.
[104] De Cagna F, Fusar-Poli L, Damiani S, Rocchetti M, Giovanna G, Mori A, Politi P and Brondino N. The role of intranasal oxytocin in anxiety and depressive disorders: a systematic review of randomized controlled trials. Clin Psychopharmacol Neurosci 2019; 17: 1-11.
[105] Horta M, Kaylor K, Feifel D and Ebner NC. Chronic oxytocin administration as a tool for investigation and treatment: a cross-disciplinary systematic review. Neurosci Biobehav Rev 2019; 108: 1-23.
[106] Craft S, Claxton A, Baker LD, Hanson AJ, Cholerton B, Trittschuh EH, Dahl D, Caulder E, Neth B, Montine TJ, Jung Y, Maldjian J, Whitlow C and Friedman S. Effects of regular and long-acting insulin on cognition and Alzheimer's disease biomarkers: a pilot clinical trial. J Alzheimers Dis 2017; 57: 1325-1334.
[107] Kullmann S, Heni M, Veit R, Scheffler K, Machann J, Haring HU, Fritsche A and Preissl H. Selective insulin resistance in homeostatic and cognitive control brain areas in overweight and obese adults. Diabetes Care 2015; 38: 1044-1050.
[108] Wingrove J, Swedrowska M, Scherließ R, Parry M, Ramjeeawon M, Taylor D, Gauthier G, Brown L, Amiel S, Zelaya F and Forbes B. Characterisation of nasal devices for delivery of insulin to the brain and evaluation in humans using functional magnetic resonance imaging. J Control Release 2019; 302: 140-147.
[109] Kumar J, Völlm B and Palaniyappan L. Oxytocin affects the connectivity of the precuneus and the amygdala: a randomized, double-blinded, placebo-controlled neuroimaging trial. Int J Neuropsychopharmacol 2014; 18.
[110] Grace SA, Labuschagne I, Castle DJ and Rossell SL. Intranasal oxytocin alters amygdala-temporal resting-state functional connectivity in body dysmorphic disorder: a double-blind placebo-controlled randomized trial. Psychoneuroendocrinology 2019; 107: 179-186.
[111] da Fonseca CO, Linden R, Futuro D, Gattass CR and Quirico-Santos T. Ras pathway activation in gliomas: a strategic target for intranasal administration of perillyl alcohol. Arch Immunol Ther Exp (Warsz) 2008; 56: 267-276.
[112] Jones T. The imaging science of positron emission tomography. Eur J Nucl Med 1996; 23: 807-813.
[113] Bushberg JT, Seibert JA, Boone JM and Leidholdt EM. The essential physics of medical imaging. Williams & Wilkins 2012.

[114] Vasdev N and Alavi A. Novel PET radiotracers with potential clinical applications. PET Clin 2017; 12: xi-xii.
[115] Jones T and Townsend D. History and future technical innovation in positron emission tomography. J Med Imaging (Bellingham) 2017; 4: 011013.
[116] Vaquero JJ and Kinahan P. Positron emission tomography: current challenges and opportunities for technological advances in clinical and preclinical imaging systems. Annu Rev Biomed Eng 2015; 17: 385-414.
[117] Nievelstein RA, Quarles van Ufford HM, Kwee TC, Bierings MB, Ludwig I, Beek FJ, de Klerk JM, Mali WP, de Bruin PW and Geleijns J. Radiation exposure and mortality risk from CT and PET imaging of patients with malignant lymphoma. Eur Radiol 2012; 22: 1946-1954.
[118] Zhu A, Lee D and Shim H. Metabolic positron emission tomography imaging in cancer detection and therapy response. Semin Oncol 2011; 38: 55-69.
[119] Couvineau A, Voisin T, Nicole P, Gratio V, Abad C and Tan YV. Orexins as novel therapeutic targets in inflammatory and neurodegenerative diseases. Front Endocrinol (Lausanne) 2019; 10: 709.
[120] Dhuria SV, Hanson LR and Frey WH 2nd. Intranasal drug targeting of hypocretin-1 (orexin-A) to the central nervous system. J Pharm Sci 2009; 98: 2501-2515.
[121] Van de Bittner GC, Van de Bittner KC, Wey HY, Rowe W, Dharanipragada R, Ying X, Hurst W, Giovanni A, Alving K, Gupta A, Hoekman J and Hooker JM. Positron emission tomography assessment of the intranasal delivery route for orexin A. ACS Chem Neurosci 2018; 9: 358-368.
[122] Yuki Y, Nochi T, Harada N, Katakai Y, Shibata H, Mejima M, Kohda T, Tokuhara D, Kurokawa S, Takahashi Y, Ono F, Kozaki S, Terao K, Tsukada H and Kiyono H. In vivo molecular imaging analysis of a nasal vaccine that induces protective immunity against botulism in nonhuman primates. J Immunol 2010; 185: 5436-5443.
[123] Shingaki T, Katayama Y, Nakaoka T, Irie S, Onoe K, Okauchi T, Hayashinaka E, Yamaguchi M, Tanki N, Ose T, Hayashi T, Wada Y, Furubayashi T, Cui Y, Sakane T and Watanabe Y. Visualization of drug translocation in the nasal cavity and pharmacokinetic analysis on nasal drug absorption using positron emission tomography in the rat. Eur J Pharm Biopharm 2016; 99: 45-53.
[124] Singh N, Veronese M, O'Doherty J, Sementa T, Bongarzone S, Cash D, Simmons C, Arcolin M, Marsden PK, Gee A and Turkheimer FE. Assessing the feasibility of intranasal radiotracer administration for in brain PET imaging. Nucl Med Biol 2018; 66: 32-39.
[125] Craft S, Baker LD, Montine TJ, Minoshima S, Watson GS, Claxton A, Arbuckle M, Callaghan M, Tsai E, Plymate SR, Green PS, Leverenz J, Cross D and Gerton B. Intranasal insulin therapy for Alzheimer disease and amnestic mild cognitive impairment: a pilot clinical trial. Arch Neurol 2012; 69: 29-38.
[126] Mottolese R, Redoute J, Costes N, Le Bars D and Sirigu A. Switching brain serotonin with oxytocin. Proc Natl Acad Sci U S A 2014; 111: 8637-8642.
[127] White ND. Increasing Naloxone access and use to prevent opioid overdose death and disability. Am J Lifestyle Med 2019; 13: 33-35.
[128] Johansson J, Hirvonen J, Lovro Z, Ekblad L, Kaasinen V, Rajasilta O, Helin S, Tuisku J, Siren S, Pennanen M, Agrawal A, Crystal R, Vainio PJ, Alho H and Scheinin M. Intranasal naloxone rapidly occupies brain mu-opioid receptors in human subjects. Neuropsychopharmacology 2019; 44: 1667-1673.
[129] Spencer CM, Gunasekara NS and Hills C. Zolmitriptan: a review of its use in migraine. Drugs 1999; 58: 347-374.
[130] Tepper SJ, Chen S, Reidenbach F and Rapoport AM. Intranasal zolmitriptan for the treatment of acute migraine. Headache 2013; 53 Suppl 2: 62-71.
[131] Yates R, Sorensen J, Bergstrom M, Antoni G, Nairn K, Kemp J, Langstrom B and Dane A. Distribution of intranasal C-zolmitriptan assessed by positron emission tomography. Cephalalgia 2005; 25: 1103-1109.
[132] Kwok PCL, Wallin M, Dolovich MB and Chan HK. Studies of radioaerosol deposition in the respiratory tract. Semin Nucl Med 2019; 49: 62-70.
[133] Esposito E, Boschi A, Ravani L, Cortesi R, Drechsler M, Mariani P, Moscatelli S, Contado C, Di Domenico G, Nastruzzi C, Giganti M and Uccelli L. Biodistribution of nanostructured lipid carriers: a tomographic study. Eur J Pharm Biopharm 2015; 89: 145-156.
[134] Mandlik SK, Ranpise NS, Mohanty BS and Chaudhari PR. A coupled bimodal SPECT-CT imaging and brain kinetics studies of zolmitriptan-encapsulated nanostructured polymeric carriers. Drug Deliv Transl Res 2018; 8: 797-805.
[135] Shiga H, Taki J, Yamada M, Washiyama K, Amano R, Matsuura Y, Matsui O, Tatsutomi S, Yagi S, Tsuchida A, Yoshizaki T, Furukawa M, Kinuya S and Miwa T. Evaluation of the olfactory nerve transport function by SPECT-MRI fusion image with nasal thallium-201 administration. Mol Imaging Biol 2011; 13: 1262-1266.

[136] Shiga H, Taki J, Washiyama K, Yamamoto J, Kinase S, Okuda K, Kinuya S, Watanabe N, Tonami H, Koshida K, Amano R, Furukawa M and Miwa T. Assessment of olfactory nerve by SPECT-MRI image with nasal thallium-201 administration in patients with olfactory impairments in comparison to healthy volunteers. PLoS One 2013; 8: e57671.
[137] Jafarieh O, Md S, Ali M, Baboota S, Sahni JK, Kumari B, Bhatnagar A and Ali J. Design, characterization, and evaluation of intranasal delivery of ropinirole-loaded mucoadhesive nanoparticles for brain targeting. Drug Dev Ind Pharm 2015; 41: 1674-1681.
[138] Sharma D, Maheshwari D, Philip G, Rana R, Bhatia S, Singh M, Gabrani R, Sharma SK, Ali J, Sharma RK and Dang S. Formulation and optimization of polymeric nanoparticles for intranasal delivery of lorazepam using Box-Behnken design: in vitro and in vivo evaluation. Biomed Res Int 2014; 2014: 156010.
[139] Patel S, Chavhan S, Soni H, Babbar AK, Mathur R, Mishra AK and Sawant K. Brain targeting of risperidone-loaded solid lipid nanoparticles by intranasal route. J Drug Target 2011; 19: 468-474.
[140] Kakkar V, Mishra AK, Chuttani K and Kaur IP. Proof of concept studies to confirm the delivery of curcumin loaded solid lipid nanoparticles (C-SLNs) to brain. Int J Pharm 2013; 448: 354-359.
[141] Casettari L and Illum L. Chitosan in nasal delivery systems for therapeutic drugs. J Control Release 2014; 190: 189-200.
[142] Djupesland PG, Messina JC and Mahmoud RA. Breath powered nasal delivery: a new route to rapid headache relief. Headache 2013; 53 Suppl 2: 72-84.
[143] Earnest FT, Baker HL Jr, Kispert DB and Laws ER Jr. Magnetic resonance imaging vs. computed tomography: advantages and disadvantages. Clin Neurosurg 1985; 32: 540-573.
[144] Goldman LW. Principles of CT and CT technology. J Nucl Med Technol 2007; 35: 115-128; quiz 129-130.
[145] Srikala Narayanan WAKAaST. In: Elsevier I, editor. Zitelli and Davis' Atlas of Pediatric Physical Diagnosis. 2018. pp. 916-990.
[146] De Backer JW, Vos WG, Burnell P, Verhulst SL, Salmon P, De Clerck N and De Backer W. Study of the variability in upper and lower airway morphology in Sprague-Dawley rats using modern micro-CT scan-based segmentation techniques. Anat Rec (Hoboken) 2009; 292: 720-727.
[147] Casteleyn C, Cornillie P, Hermens A, Van Loo D, Van Hoorebeke L, van den Broeck W and Simoens P. Topography of the rabbit paranasal sinuses as a prerequisite to model human sinusitis. Rhinology 2010; 48: 300-304.
[148] Warnken ZN, Smyth HDC, Davis DA, Weitman S, Kuhn JG and Williams RO 3rd. Personalized medicine in nasal delivery: the use of patient-specific administration parameters to improve nasal drug targeting using 3D-printed nasal replica casts. Mol Pharm 2018; 15: 1392-1402.
[149] Frank DO, Kimbell JS, Cannon D and Rhee JS. Computed intranasal spray penetration: comparisons before and after nasal surgery. Int Forum Allergy Rhinol 2013; 3: 48-55.
[150] Engelhardt L, Rohm M, Mavoungou C, Schindowski K, Schafmeister A and Simon U. First steps to develop and validate a CFPD model in order to support the design of nose-to-brain delivered biopharmaceuticals. Pharm Res 2016; 33: 1337-1350.
[151] Shang Y, Inthavong K and Tu J. Development of a computational fluid dynamics model for mucociliary clearance in the nasal cavity. J Biomech 2019; 85: 74-83.
[152] Carvalho LA, Teng J, Fleming RL, Tabet EI, Zinter M, de Melo Reis RA and Tannous BA. Olfactory ensheathing cells: a trojan horse for glioma gene therapy. J Natl Cancer Inst 2019; 111: 283-291.
[153] Ji G, Liu M, Zhao XF, Liu XY, Guo QL, Guan ZF, Zhou HG and Guo JC. NF-kappaB signaling is involved in the effects of intranasally engrafted human neural stem cells on neurofunctional improvements in neonatal rat hypoxic-ischemic encephalopathy. CNS Neurosci Ther 2015; 21: 926-935.
[154] Thompson JM and Miller LS. Preclinical optical imaging to study pathogenesis, novel therapeutics and diagnostics against orthopaedic infection. J Orthop Res 2019; 37: 2269-2277.
[155] Yan Y, Shi P, Song W and Bi S. Chemiluminescence and bioluminescence imaging for biosensing and therapy: in vitro and in vivo perspectives. Theranostics 2019; 9: 4047-4065.
[156] Tai PA, Liu YL, Wen YT, Lin CM, Huynh TT, Hsiao M, Wu ATH and Wei L. The development and applications of a dual optical imaging system for studying glioma stem cells. Mol Imaging 2019; 18: 1536012119870899.
[157] Gil CJ, Tomov ML, Theus AS, Cetnar A, Mahmoudi M and Serpooshan V. In vivo tracking of tissue engineered constructs. Micromachines 2019; 10: 474.
[158] Yeh HW, Karmach O, Ji A, Carter D, Martins-Green MM and Ai HW. Red-shifted luciferase-luciferin pairs for enhanced bioluminescence imaging. Nat Methods 2017; 14: 971-974.
[159] England CG, Ehlerding EB and Cai W. NanoLuc: a small luciferase is brightening up the field of

bioluminescence. Bioconjug Chem 2016; 27: 1175-1187.
[160] Bagheri-Mohammadi S, Alani B, Karimian M, Moradian-Tehrani R and Noureddini M. Intranasal administration of endometrial mesenchymal stem cells as a suitable approach for Parkinson's disease therapy. Mol Biol Rep 2019; 46: 4293-4302.
[161] Chou LY and Chan WC. Fluorescence-tagged gold nanoparticles for rapidly characterizing the size-dependent biodistribution in tumor models. Adv Healthc Mater 2012; 1: 714-721.
[162] Zhang Y, Yu J, Kahkoska AR and Gu Z. Photoacoustic drug delivery. Sensors (Basel) 2017; 17.
[163] Xu M and Wang L. Photoacoustic imaging in biomedicine. Rev Sci Instrum 2006; 77.
[164] Wang D, Wu Y and Xia J. Review on photoacoustic imaging of the brain using nanoprobes. Neurophotonics 2016; 3: 010901.
[165] Huang L, Ao L, Hu D, Wang W, Sheng Z and Su W. Magneto-plasmonic nanocapsules for multimodal-imaging and magnetically guided combination cancer therapy. Chem Mater 2016; 28: 5896-5904.
[166] Chen H, Chen CC, Acosta C, Wu SY, Sun T and Konofagou EE. A new brain drug delivery strategy: focused ultrasound-enhanced intranasal drug delivery. PLoS One 2014; 9: e108880.
[167] Ye D, Zhang X, Yue Y, Raliya R, Biswas P, Taylor S, Tai YC, Rubin JB, Liu Y and Chen H. Focused ultrasound combined with microbubble-mediated intranasal delivery of gold nanoclusters to the brain. J Control Release 2018; 286: 145-153.